

Peripheral transverse densities of the baryon octet from chiral effective field theory and dispersion analysis

J. M. Alarcón^{a,b}, A. N. Hiller Blin^c, M. J. Vicente Vacas^c, C. Weiss^b

^aHelmholtz-Institut für Strahlen- und Kernphysik & Bethe Center for Theoretical Physics, Universität Bonn, 53115 Bonn, Germany

^bTheory Center, Jefferson Lab, Newport News, VA 23606, USA

^cDepartamento de Física Teórica and IFIC, Centro Mixto Universidad de Valencia-CSIC, Institutos de Investigación de Paterna, E-46071 Valencia, Spain

Abstract

The baryon electromagnetic form factors are expressed in terms of two-dimensional densities describing the distribution of charge and magnetization in transverse space at fixed light-front time. We calculate the transverse densities of the spin-1/2 flavor-octet baryons at peripheral distances $b = \mathcal{O}(M_\pi^{-1})$ using methods of relativistic chiral effective field theory (χ EFT) and dispersion analysis. The densities are represented as dispersive integrals over the imaginary parts of the form factors in the timelike region (spectral functions). The isovector spectral functions on the two-pion cut $t > 4M_\pi^2$ are calculated using relativistic χ EFT including octet and decuplet baryons. The χ EFT calculations are extended into the ρ meson mass region using an N/D method that incorporates the pion electromagnetic form factor data. The isoscalar spectral functions are modeled by vector meson poles. We compute the peripheral charge and magnetization densities in the octet baryon states, estimate the uncertainties, and determine the quark flavor decomposition. The approach can be extended to baryon form factors of other operators and the moments of generalized parton distributions.

Keywords: Electromagnetic form factors, chiral lagrangians, dispersion relations, hyperons, charge distribution

PACS: 12.40.Vv, 13.40.Gp, 11.55.Fv, 13.60.Hb

1. Introduction

Exploring the spatial structure of hadrons and their interactions is a central objective of modern strong interaction physics. The description of hadrons as extended objects in relativistic space-time enables an intuitive understanding of their structure and permits the formulation of novel approximation methods based on physical distance scales. The most basic information about spatial structure comes from the transition matrix elements (or form factors) of electroweak current operators, which reveal the distributions of charge and current in the system. In non-relativistic systems, such as nuclei in nuclear many-body theory, the form factors are represented as the Fourier transform of 3-dimensional spatial distributions of charge and current at a fixed instant of time $x^0 = \text{const}$. These distributions can be related to probability densities of the N -particle Schrödinger wave function. In relativistic systems such as hadrons the formulation of a density requires separating the structure of the “system” from that of the “probe” in the presence of vacuum fluctuations that change the number of constituents. This is accomplished in a frame-independent manner by viewing the system at fixed light-front time $x^+ = x^0 + x^3$ (light-front quantization) [1, 2, 3, 4]. In this framework the form factors are represented in terms of 2-dimensional spatial distributions of charge and current at fixed light-front time $x^+ = \text{const}$. [5, 6, 7, 8]. The transverse densities are frame-independent (they remain invariant under longitudinal boosts and transform kinematically under transverse boosts) and provide an objective spa-

tial representation of the hadron as a relativistic system. The properties of the transverse densities of mesons and baryons, their extraction from experimental data, and their explanation in dynamical models have been discussed extensively in the literature [8, 9, 10, 11, 12]; see Ref. [13] for a review. An important aspect is that the transverse densities are naturally related to the partonic structure of hadrons probed in high-energy short-distance processes (generalized parton distributions, or GPDs). The densities describe the cumulative charge and current carried by the quarks/antiquarks in the hadron at a given transverse position and represent the integral of the GPDs over the quark/antiquark light-front momentum fraction [6, 7, 14]; see Refs. [15, 16] for a review. This relation places the study of elastic form factors in the context of exploring the 3-dimensional quark-gluon structure of hadrons in QCD.

Of particular interest are the transverse densities at distances of the order $b = \mathcal{O}(M_\pi^{-1})$, where the pion mass is regarded as parametrically small on the hadronic mass scale (as represented e.g. by the vector meson mass M_V) [17, 18]. At such “peripheral” distances the densities are governed by the effective dynamics resulting from the spontaneous breaking of chiral symmetry and can be computed model-independently using methods of chiral effective field theory (χ EFT) [19, 20]; see Refs. [21, 22, 23] for a review. The peripheral densities are generated by chiral processes in which the hadron couples to the current operator through soft-pion exchange in the t -channel. The nucleon’s peripheral charge and magnetization densities

(related to the electromagnetic form factors F_1 and F_2) were studied in Ref. [18] using relativistic χ EFT in the leading-order approximation. The densities decay exponentially at large b with a range of the order $1/(2M_\pi)$, and exhibit a rich structure due to the coupling of the two-pion exchange to the nucleon. It was found that the peripheral charge and current densities are similar in magnitude and related by an approximate inequality. These properties are a consequence of the essentially relativistic nature of chiral dynamics [the typical pion momenta are $\mathcal{O}(M_\pi)$] and can be understood in a simple quantum-mechanical picture of peripheral nucleon structure [24, 25, 26]. It was also shown that the χ EFT densities exhibit the correct N_c -scaling behavior if contributions from Δ isobar intermediate states are included [18, 26].

The study of peripheral transverse densities is closely connected with the dispersive representation of the nucleon form factors. The form factors are analytic functions of the invariant momentum transfer t and can be represented as dispersive integrals of their imaginary parts (spectral functions) on the two-pion cut at timelike $t > 4M_\pi^2$. The integration extends over the unphysical region below the nucleon-antinucleon threshold, where the spectral functions cannot be measured directly, but can be calculated theoretically using χ EFT [27, 28, 29, 30, 31] and dispersion theory [32, 33, 34, 35, 36], or determined by fits to the spacelike form factor data [37, 38, 39]. The transverse densities are given by similar dispersive integrals, in which the spectral functions are integrated with an exponential weight factor $\sim \exp(-b\sqrt{t})$, suppressing the contribution from large masses [17, 40]. At distances $b = \mathcal{O}(M_\pi^{-1})$ the integration is limited to the near-threshold region $t - 4M_\pi^2 = \mathcal{O}(M_\pi^2)$, where the spectral functions are governed by chiral dynamics. The peripheral densities thus represent “clean” chiral observables and are ideally suited for χ EFT calculations. Quantitative studies in Ref. [40] found that at distances $b > 3$ fm the dispersive integrals for the densities are dominated by the region $4M_\pi^2 < t \lesssim 10M_\pi^2$, where the isovector spectral functions can be computed directly using fixed-order χ EFT. To obtain the densities at smaller distances $b \sim 1$ fm one needs to construct the spectral functions at larger values of t , where they are affected by strong $\pi\pi$ rescattering in the t -channel and the ρ meson resonance at $t \sim M_\rho^2 = 30M_\pi^2$. This can be accomplished in an approach that combines χ EFT with a dispersive technique based on elastic unitarity in the t -channel.

In this article we study the peripheral transverse densities of the spin-1/2 flavor-octet baryons using methods of χ EFT and dispersive analysis. We calculate the spectral functions of the isovector electromagnetic form factors on the two-pion cut at $t > 4M_\pi^2$, using relativistic χ EFT with $SU(3)$ flavor group and explicit spin-3/2 decuplet degrees of freedom at $\mathcal{O}(\epsilon^3)$ in the small-scale expansion. The calculations are extended from the near-threshold region to masses $t \sim 16M_\pi^2$ and higher, using a dispersive technique that incorporates $\pi\pi$ rescattering through elastic unitarity and the pion electromagnetic form factor data. The method allows us to compute the isovector transverse densities at distances $b \gtrsim 1$ fm with controlled uncertainties. For the isoscalar densities we construct an empirical parametrization of the spectral function in terms of vector meson poles

(ω, ϕ) using $SU(3)$ symmetry. We present the isovector and isoscalar peripheral transverse densities of the individual octet baryons and discuss their properties. We also calculate the flavor decomposition of the peripheral densities and compare it to the baryons’ valence quark content.

The treatment of spectral functions and transverse densities presented here goes beyond that of previous studies in several aspects. First, the χ EFT calculations are performed with the $SU(3)$ flavor group, which allows us to study for the first time the peripheral densities of all octet baryons resulting from two-pion exchange in the t -channel (contributions from two-kaon exchange are included as well but turn out to be negligible at peripheral distances). Second, the spin-3/2 decuplet baryons are included in the χ EFT calculations using a consistent Lagrangian, which eliminates off-shell effects in physical observables. This approach, together with a fully relativistic formulation of χ EFT with baryons via the extended-on-mass-shell (or EOMS) scheme [41], overcomes certain specific difficulties that arise in χ EFT calculations of fundamental processes [42, 43, 44, 45, 46] and has been applied successfully to the form factors of the nucleon and the Δ isobar [47], the magnetic moments of the octet and decuplet baryons [48], the axial-vector charge of the octet [49], and to the calculation of quantities like the nucleon σ -terms and two photon exchange corrections to the muonic hydrogen Lamb shift [50, 51, 52], which are used in searches of physics beyond the standard model. Earlier χ EFT calculations of peripheral densities [18, 26] included the Δ isobar through a “minimal” $\pi N \Delta$ coupling with off-shell dependence; this scheme was sufficient to achieve proper N_c -scaling of the spectral functions and densities, but could not fix the contact terms associated with the isobar contribution; see Ref. [18, 26] for details.

Third, we extend the range of the χ EFT calculation of the spectral function beyond the near-threshold region by combining it with a dispersive method based on elastic unitarity. It uses the representation of the spectral functions on the two-pion cut as the product of the $\pi\pi \rightarrow B\bar{B}$ t -channel partial-wave amplitudes in the $I = J = 1$ channel, $\Gamma_i^B(t)$ ($i = 1, 2$), and the complex-conjugate pion form factor, $F_\pi^*(t)$. Chiral EFT is used to calculate the real function $\Gamma_i^B(t)/F_\pi(t)$ ($i = 1, 2$), in which the common phase due to $\pi\pi$ rescattering cancels by virtue of the Watson theorem [32, 33, 34, 53]; the result is then multiplied by the empirical $|F_\pi(t)|^2$ measured in e^+e^- annihilation experiments, which contains the $\pi\pi$ rescattering effects and the ρ resonance. The “improved” χ EFT spectral functions thus obtained agree well with the empirical spectral functions (obtained by analytic continuation of the partial wave amplitudes) [37, 35] up to $t \sim 16M_\pi^2$ and have qualitatively correct behavior even in the ρ meson mass region. The agreement is achieved without adding free parameters and represents a genuine prediction of χ EFT at $\mathcal{O}(\epsilon^3)$; the inclusion of higher-order chiral corrections might further improve the accuracy of the results in the ρ meson mass region. The method allows us to compute the isovector transverse densities down to distances $b \sim 1$ fm with controlled accuracy and results in a major overall improvement in the description of peripheral nucleon structure. The method could be extended to the spectral functions of other form fac-

tors with two-pion cut and their transverse densities [54]. The technique described here is a variant of the N/D method of amplitude analysis [55], which was employed in applications of χ EFT to meson-meson, meson-baryon, and baryon-baryon scattering [43, 56, 57, 58, 59, 60, 61]. A similar approach was used in a recent study of the Σ - Λ transition form factors [62].

The article is structured as follows. In Sec. 2 we summarize the basic properties of the transverse densities and discuss their dispersive representation. In particular, we analyze the distribution of strength in the dispersion integral for the densities at different distances and identify the regions of t where we need to calculate the spectral functions. In Sec. 3 we describe the χ EFT calculation of the isovector spectral functions, the improvement using dispersion theory, and the modeling of isoscalar spectral functions. In Sec. 4 we present the results for the charge and magnetization densities of the octet baryons and discuss their properties. We also perform the flavor separation of the transverse densities and discuss the connection with partonic structure. A summary and outlook on further studies are given in Sec. 5. Technical material is collected in the appendices. Appendix A describes the validation of the form factor calculations. Appendix B discusses the role of the off-shell behavior of the χ EFT with Δ isobars and compares our results with previous calculations. Appendix C describes our model for the coupling of isoscalar vector mesons to the $SU(3)$ octet baryons. Preliminary results of the present study were reported in Ref. [63].

2. Transverse densities

2.1. Form factors and transverse densities

The transition matrix element of the electromagnetic current between states of a spin-1/2 baryon B with 4-momenta p and p' is of the general form

$$\langle B(p') | J^\mu | B(p) \rangle = \bar{u}(p') \left[\gamma^\mu F_1^B(t) + \frac{i\sigma^{\mu\nu}\Delta_\nu}{2m_B} F_2^B(t) \right] u(p), \quad (1)$$

where $u(p)$ and $\bar{u}(p')$ are the Dirac spinors of the baryon states, m_B is the baryon mass, $\Delta = p' - p$ is the 4-momentum transfer, and $\sigma^{\mu\nu} = (i/2)[\gamma^\mu, \gamma^\nu]$. The form factors $F_1^B(t)$ and $F_2^B(t)$ (Dirac and Pauli form factor) are functions of the Lorentz-invariant momentum transfer $t = \Delta^2$, with $t < 0$ in the physical region of elastic scattering. They are invariant functions and can be measured and interpreted without specifying the form of relativistic dynamics or choosing a reference frame. The isospin decomposition of Eq. (1) in the case of $SU(3)$ octet baryons ($B = N, \Lambda, \Sigma, \Xi$) will be described below.

In the light-front form of relativistic dynamics one considers the evolution of strong interactions in light-front time $x^+ \equiv x^0 + x^3 = x^0 + z$. The baryon states are parametrized by their light-front momentum $p^+ \equiv p^0 + p^z$ and transverse momentum $\mathbf{p}_T \equiv (p^x, p^y)$, whereas $p^- \equiv p^0 - p^z$ plays the role of the energy, with $p^- = (p_T^2 + m_B^2)/p^+$ on the baryon mass shell $p^2 = m_B^2$. In this context one naturally considers the current matrix element in a class of reference frames where the momentum transfer has only transverse components, $\Delta^+ = \Delta^- = 0$, $\Delta_T \neq 0$, $|\Delta_T|^2 = -t$.

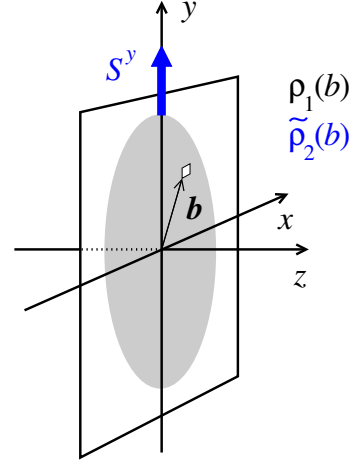


Figure 1: Interpretation of the baryon transverse densities, cf. Eq. (1). The function $\rho_1(b)$ describes the spin-independent part of the expectation value of the J^+ current in a baryon state localized at the transverse origin. The function $\cos \phi \tilde{\rho}_2(b)$ describes the spin-dependent part of the current in a state polarized in the positive y -direction.

The form factors are then represented as Fourier transforms of two-dimensional spatial densities (transverse densities)

$$F_i^B(t = -|\Delta_T|^2) = \int d^2b e^{i\Delta_T \cdot b} \rho_i^B(b) \quad (i = 1, 2), \quad (2)$$

where $\mathbf{b} \equiv (b^x, b^y)$ is a transverse coordinate variable and $b \equiv |\mathbf{b}|$; we follow the conventions of Ref. [18]. The spatial integral of the densities reproduces the total charge and anomalous magnetic moment of the baryons,

$$\int d^2b \rho_1^B(b) = F_1^B(0) = Q^B, \quad (3)$$

$$\int d^2b \rho_2^B(b) = F_2^B(0) = \kappa^B. \quad (4)$$

The functions thus describe the transverse spatial distribution of charge and magnetization in the baryon. The interpretation of $\rho_1^B(b)$ and $\rho_2^B(b)$ as spatial densities has been discussed extensively in the literature [6, 7, 13] and is summarized in Ref. [18]. In a state where the baryon is localized in transverse space at the origin, and its spin (or light-front helicity) quantized in the y -direction, the expectation value of the current $J^+(x)$ at $x^+ = x^- = 0$ and transverse position $\mathbf{x}_T = \mathbf{b}$ is given by

$$\langle J^+(\mathbf{b}) \rangle_{\text{localized}} = (\dots) \left[\rho_1^B(b) + (2S^y) \cos \phi \tilde{\rho}_2^B(b) \right], \quad (5)$$

$$\tilde{\rho}_2^B(b) \equiv \frac{\partial}{\partial b} \left[\frac{\rho_2^B(b)}{2m_B} \right]. \quad (6)$$

Here (...) represents a factor resulting from the normalization of states (see Ref. [18] for details), ϕ is the angle of the vector \mathbf{b} relative to the x -axis, and $S^y = \pm 1/2$ is the spin projection in the y -direction in the baryon rest frame (see Fig. 1). $\rho_1^B(b)$ describes the spin-independent part of the plus current in

a localized baryon state, while $\cos\phi\bar{\rho}_2^B(b)$ describes the spin-dependent part of the current in a transversely polarized baryon. Other aspects of the transverse densities, such as their connection with the partonic structure and GPDs, are discussed in the literature and reviewed in Ref. [13].

In the present work the concepts of light-front quantization are used only for the interpretation of the transverse densities but will not be employed in the actual calculations. Dynamical calculations (chiral EFT, dispersion theory) will be performed at the level of the invariant form factors, from which the densities can be obtained by inverting the Fourier transform of Eq. (2). The advantage of transverse densities is precisely that they connect light-front structure with the invariant form factors, for which well-tested theoretical methods are available. An alternative approach, in which dynamical calculations in chiral EFT are performed directly in light-front quantization, is described in Refs. [24, 25, 26].

2.2. Dispersive representation

The baryon form factors are analytic functions of t , with singularities (branch points, poles) on the positive real axis. Assuming power-like asymptotic behavior $F_i^B(t) \sim t^{-(i+1)}$ ($i = 1, 2$), as expected in perturbative QCD and supported by present experimental data for the nucleon, the form factors satisfy unsubtracted dispersion relations of the form

$$F_i^B(t) = \int_{t_{\text{thr}}}^{\infty} \frac{dt'}{t' - t - i0} \frac{\text{Im} F_i^B(t')}{\pi} \quad (i = 1, 2). \quad (7)$$

Here the form factors are expressed as integrals of their imaginary parts (or spectral functions) on the principal cut on the physical sheet. The singularities at $t > t_{\text{thr}}$ correspond to processes in which the current produces a hadronic state that couples to the baryon-antibaryon system, current \rightarrow hadronic state $\rightarrow B\bar{B}$ (see Fig. 2). The hadronic state with the lowest mass is the two-pion state with threshold at $t_{\text{thr}} = 4M_\pi^2$, produced by the isovector current (anomalous thresholds with $t_{\text{thr}} < 4M_\pi^2$ in the strange octet baryon form factors will be discussed in Sec. 3.2). At larger values $t \lesssim 1 \text{ GeV}^2$ the dominant states are the vector mesons appearing as resonances in the two-pion channel (ρ , isovector) and the three-pion channel (ω , isoscalar). At even higher t the spectral functions receive contributions from $K\bar{K}$ states and the ϕ resonance, and from other multi-hadron states whose composition is not known in detail. Most of the relevant states lie below the $B\bar{B}$ threshold ($t = 4m_N^2 = 3.5 \text{ GeV}^2$ for the nucleon), in the unphysical region of the current $\rightarrow B\bar{B}$ process, where the spectral functions cannot be measured directly in conversion experiments, but can only be calculated theoretically. Methods for constructing the spectral functions in different regions of t (χ EFT, dispersion analysis) will be described below.

A similar dispersive representation can be derived for the transverse densities associated with the form factors, Eq. (2). Calculating the transverse Fourier transform of the form factors as given by Eq. (7), and using Eq. (6), one obtains [17, 40]

$$\rho_1^B(b) = \int_{t_{\text{thr}}}^{\infty} dt \frac{K_0(\sqrt{tb})}{2\pi} \frac{\text{Im} F_1^B(t)}{\pi}, \quad (8)$$

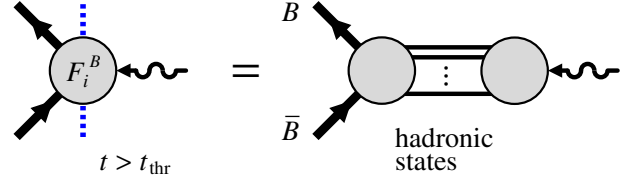


Figure 2: Spectral function of the baryon form factors.

$$\bar{\rho}_2^B(b) = - \int_{t_{\text{thr}}}^{\infty} dt \frac{\sqrt{t} K_1(\sqrt{tb})}{2\pi} \frac{\text{Im} F_2^B(t)}{\pi}, \quad (9)$$

where $K_n(z)$ ($n = 0, 1$) denotes the modified Bessel functions of the second kind. This representation has several interesting properties. (a) The modified Bessel functions decay exponentially at large arguments,

$$K_n(\sqrt{tb}) \sim [\pi/(2\sqrt{tb})]^{1/2} e^{-\sqrt{tb}} \quad (\sqrt{tb} \gg 1). \quad (10)$$

The dispersive integrals for the densities therefore converge exponentially at large t , while the original integrals for the form factors converge only like a power. This greatly reduces the contribution from the high-mass region where the spectral functions are poorly known. (b) The density at a certain b is given by the integral of the spectral function with the “exponential filter” $K_n(\sqrt{tb})$. The distance b therefore represents an external parameter that allows one to effectively select (emphasize or de-emphasize) certain mass regions in the spectral function. The large-distance behavior of the densities is governed by the lowest-mass states in a given channel. We shall use this property to identify the region of b in which the densities are dominated by values of t close to the two-pion threshold, where the spectral functions can be computed using χ EFT and dispersion theory. (c) The representations Eqs. (8) and (9) incorporate the correct analytic behavior of the form factors and can be used to study the large-distance asymptotics of the densities.¹

It is instructive to study the distribution of strength in t in the dispersive integrals for the baryon densities, Eqs. (8) and (9), at different b [40]. For this purpose we consider the nucleon form factors, whose isovector spectral functions at $t < 1 \text{ GeV}^2$ have been calculated using amplitude analysis techniques (analytic continuation of the $\pi\pi \rightarrow N\bar{N}$ partial-wave amplitudes [35, 37], Roy-Steiner equations [36]). Figures 3a and b show the spectral functions of the nucleon’s isovector form factors F_1^V and F_2^V obtained in Ref. [36]. One observes the rise of the spectral functions in the region above the two-pion threshold $t > 4M_\pi^2$, and the prominent role of the ρ resonance at $t \sim 30M_\pi^2 = 0.6 \text{ GeV}^2$ (the rapid variation on the right shoulder of the ρ is due to ρ - ω mixing caused by isospin breaking). Figures 3c and d show the distribution of strength in the dispersive integrals Eqs. (8) and (9), i.e., the spectral functions multiplied by $K_0(\sqrt{tb})$ and

¹Form factor representations with incorrect analytic properties in t (e.g., with artificial singularities at complex t) are principally not adequate for studying the large-distance asymptotics of the densities, even if they provide good fits to the spacelike form factor data at small $t < 0$; see Ref. [40] for a discussion.

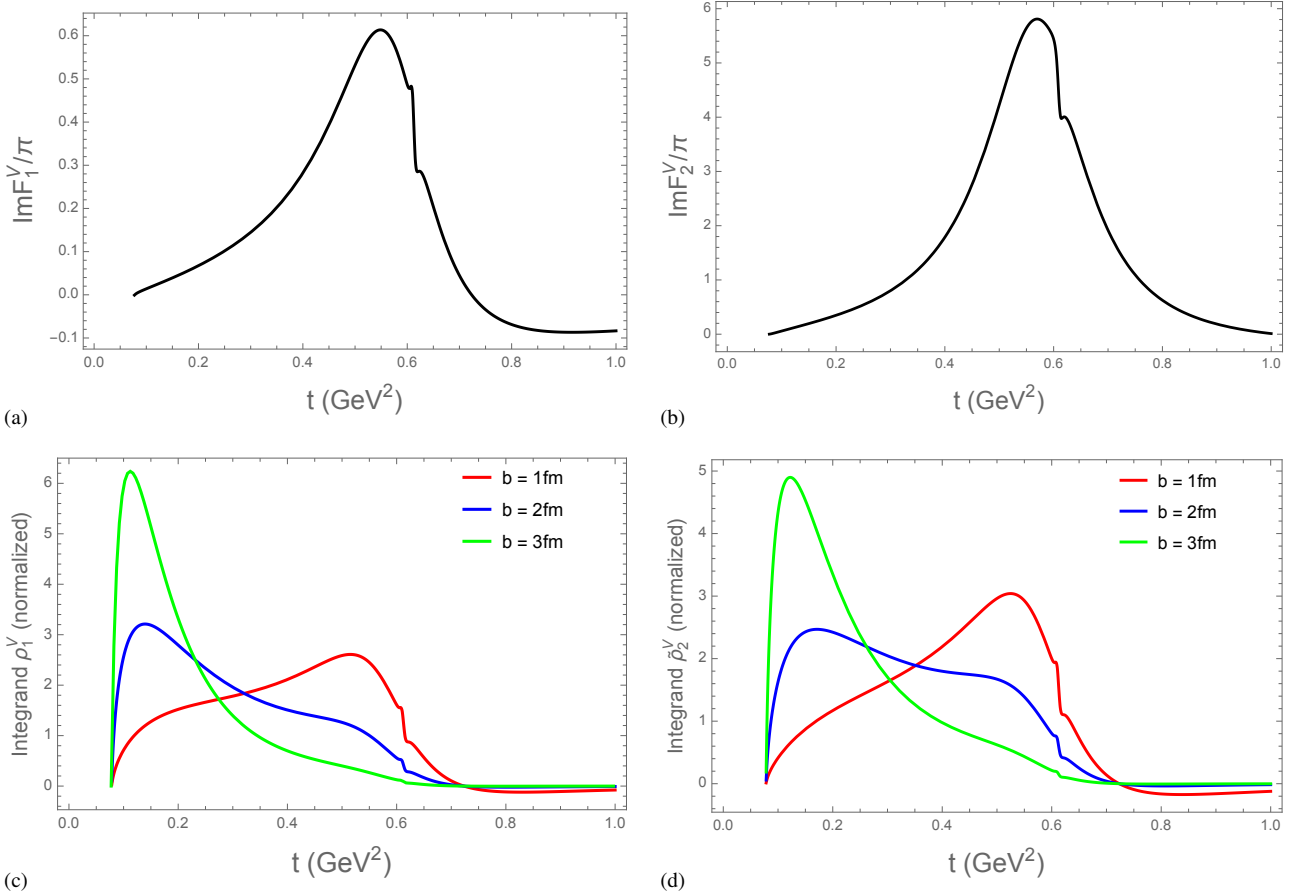


Figure 3: (a, b) Spectral functions of the nucleon isovector form factors, $\text{Im} F_1^V(t)$ and $\text{Im} F_2^V(t)$, as determined in Ref. [36]. (c, d) Distribution of strength in t in the dispersive integrals for the transverse charge density $\rho_1^V(b)$, Eq. (8), and the transverse magnetization density $\tilde{\rho}_2^V(b)$, Eq. (9), at different distances b . The plots show the integrands as functions of t , divided by the value of the integral, i.e., normalized to unit area under the curves.

$\sqrt{t}K_1(\sqrt{tb})$, for $b = 1, 2$ and 3 fm. (The plots show the distributions in t normalized to unit area under the curves, to facilitate comparison of the relative distribution of strength at different b .) One sees that for $b = 3$ fm the dominant contribution to the integrals arises from the near-threshold region $t < 0.3$ GeV^2 , while the vector meson region $t \sim 0.5$ GeV^2 is very strongly suppressed. For $b = 2$ fm the near-threshold region still gives the main contribution to the integrals, but the vector meson region becomes noticeable, especially in $\tilde{\rho}_2^V$. For $b = 1$ fm, finally, the vector meson mass region gives the main contribution to the integrals. These estimates illustrate in what regions of t we need to calculate (or model) the spectral functions in order to compute the densities at a given b , and how the uncertainties of the spectral function in the different regions affect the overall uncertainty of the densities. Similar estimates can be performed for the isoscalar densities of the nucleon and the densities of the other flavor-octet baryons, using the spectral functions calculated below.

In this work we use relativistic χ EFT to calculate the isovector spectral functions of the flavor-octet baryons on the two-pion cut. The relativistic χ EFT framework correctly implements the subthreshold singularities of the form factors on the

unphysical sheet, which result from the baryon Born terms and account for the steep rise of the isovector spectral function above threshold [27, 28, 29, 30, 31]. The inclusion of the decuplet baryons as dynamical degrees of freedom implements also the Born term singularities further removed from the physical region, which become important at larger t . To extend the χ EFT calculations of the spectral functions into the vector meson mass region we combine them with a dispersive technique that incorporates the pion form factor data from e^+e^- annihilation experiments [32, 33, 37]. In this way we construct the isovector spectral functions of the octet baryons up to $t \sim 0.3$ GeV^2 with an estimated uncertainty $< 30\%$, and up to $t \sim 1$ GeV^2 with somewhat larger uncertainty. The isoscalar spectral functions we model by phenomenological vector meson exchange (ω, ϕ). Non-resonant isoscalar contributions from kaon loops in the $SU(3)$ EFT turn out to be negligible. Altogether, these methods allow us to compute the peripheral densities of the octet baryons at distances $b \gtrsim 1$ fm with controlled accuracy.

2.3. Isospin structure

In the present study we consider the form factors and densities of baryons in the octet representation of the $SU(3)$ flavor

group. The electromagnetic current operator in QCD with 3 flavors is given by $J^\mu = e\bar{\psi}Q\gamma^\mu\psi$, where ψ is the quark field and Q the quark charge matrix,

$$Q = \text{diag}\left(\frac{2}{3}, -\frac{1}{3}, -\frac{1}{3}\right) = \frac{1}{2}\lambda^3 + \frac{1}{2\sqrt{3}}\lambda^8, \quad (11)$$

where λ^a are the Gell-Mann matrices. The term $\propto \lambda^3$ in the current transforms as an isovector under $SU(2)$ isospin rotations (V); the term $\propto \lambda^8$ transforms as an isoscalar (S), and the current can be represented as the sum of an isovector and an isoscalar current, $J^\mu = J^{\mu,V} + J^{\mu,S}$. The matrix elements of the isovector and isoscalar currents can be specified for each baryon state.

The baryons in the octet representation of $SU(3)$ form four isospin multiplets

$$\left. \begin{array}{ccc} \text{multiplet} & \text{baryons} & \text{isospin} \\ N & p, n & I = \frac{1}{2} \\ \Lambda & \Lambda & I = 0 \\ \Sigma & \Sigma^+, \Sigma^-, \Sigma^0 & I = 1 \\ \Xi & \Xi^0, \Xi^- & I = \frac{1}{2}. \end{array} \right\} \quad (12)$$

Within each multiplet we write the form factors as the sum/difference of an isoscalar and isovector component,

$$\left. \begin{array}{l} \{F_i^p, F_i^n\} = F_i^{N,S} \pm F_i^{N,V}, \\ F_i^\Lambda = F_i^{\Lambda,S}, \\ \{F_i^{\Sigma^+}, F_i^{\Sigma^-}\} = F_i^{\Sigma,S} \pm F_i^{\Sigma,V}, \\ F_i^{\Sigma^0} = F_i^{\Sigma,S}, \\ F_i^{\Lambda-\Sigma} = F_i^{\Lambda-\Sigma,V}, \\ \{F_i^{\Xi^0}, F_i^{\Xi^-}\} = F_i^{\Xi,S} \pm F_i^{\Xi,V} \\ (i = 1, 2). \end{array} \right\} \quad (13)$$

For the nucleon this corresponds to the standard definition of the isoscalar and isovector form factors as $\{F_i^{N,S}, F_i^{N,V}\} = \frac{1}{2}(F_i^p \pm F_i^n)$. The Λ form factors are pure isoscalar. In the Σ^0 form factors the isovector component is absent because the transition $|I = 1, I_3 = 0\rangle_{\text{current}} \rightarrow |I = 1, I_3 = 0\rangle_B |I = 1, I_3 = 0\rangle_{\bar{B}}$ is forbidden by isospin symmetry. The $\Lambda-\Sigma^0$ transition form factors $F_i^{\Lambda-\Sigma}$ are pure isovector. Equation (13) embodies the constraints imposed on the octet baryon form factors by isospin symmetry. The same decomposition applies to the spectral functions and the transverse densities.

3. Spectral functions

3.1. Chiral effective field theory

For the calculation of the baryon isovector spectral functions we use a manifestly Lorentz-covariant version of χ EFT with $SU(3)$ flavor group including spin-1/2 flavor-octet and spin-3/2 flavor-decuplet baryons. The pseudoscalar mesons and spin-1/2 baryons are described by fields in the $SU(3)$ octet representation (rank-2 tensors)

$$\phi = \begin{pmatrix} \frac{1}{\sqrt{2}}\pi^0 + \frac{1}{\sqrt{6}}\eta & \pi^+ & K^+ \\ \pi^- & -\frac{1}{\sqrt{2}}\pi^0 + \frac{1}{\sqrt{6}}\eta & K^0 \\ K^- & \bar{K}^0 & -\frac{2}{\sqrt{6}}\eta \end{pmatrix}, \quad (14)$$

$$B = \begin{pmatrix} \frac{1}{\sqrt{2}}\Sigma^0 + \frac{1}{\sqrt{6}}\Lambda & \Sigma^+ & p \\ \Sigma^- & -\frac{1}{\sqrt{2}}\Sigma^0 + \frac{1}{\sqrt{6}}\Lambda & n \\ \Xi^- & \Xi^0 & -\frac{2}{\sqrt{6}}\Lambda \end{pmatrix}. \quad (15)$$

The spin-3/2 baryons are described by fields in the $SU(3)$ decuplet representation (rank-3 totally symmetric tensor)

$$\left. \begin{array}{l} T^{111} = \Delta^{++}, \quad T^{112} = \frac{1}{\sqrt{3}}\Delta^+, \quad T^{122} = \frac{1}{\sqrt{3}}\Delta^0, \\ T^{222} = \Delta^-, \quad T^{113} = \frac{1}{\sqrt{3}}\Sigma^{*+}, \quad T^{123} = \frac{1}{\sqrt{6}}\Sigma^{*0}, \\ T^{223} = \frac{1}{\sqrt{3}}\Sigma^{*-}, \quad T^{133} = \frac{1}{\sqrt{3}}\Xi^{*0}, \\ T^{233} = \frac{1}{\sqrt{3}}\Xi^{*-}, \quad T^{333} = \Omega^-. \end{array} \right\} \quad (16)$$

The spin-1/2 fields B are introduced as relativistic bispinor fields (Dirac fields). The spin-3/2 fields are introduced as 4-vector-bispinor fields $T \equiv T_\mu$, which have to be subjected to relativistically covariant constraints to eliminate spurious spin-1/2 degrees of freedom. In the present formulation of the EFT the projection on spin-3/2 is implemented through the use of consistent interaction vertices (see below); i.e., the spin-1/2 degrees of freedom are allowed to propagate but are filtered out in the interaction [64, 65, 66, 67]. Electromagnetic interactions are introduced by the coupling to a 4-vector background field in the $SU(3)$ octet representation,

$$v_\mu = e\epsilon_\mu Q = e\epsilon_\mu \begin{pmatrix} \frac{2}{3} & 0 & 0 \\ 0 & -\frac{1}{3} & 0 \\ 0 & 0 & -\frac{1}{3} \end{pmatrix}. \quad (17)$$

The construction of the chiral Lagrangian with spin-3/2 fields and the formulation of a small-scale expansion have been described in Refs. [68, 69]. In the ϵ -expansion the octet-decuplet baryon mass splitting is counted at the same order as the pseudoscalar octet meson mass and momentum,

$$p, M_\phi \sim m_T - m_B \sim \epsilon, \quad (18)$$

where ϵ denotes the generic expansion parameter. The chiral order N of a diagram is given by

$$N = 4L - 2P_\phi - P_B - P_T + \sum_k kV_k, \quad (19)$$

where L is the number of loops, P_H the number of propagators of hadrons of the type H and V_k the number of vertices of a Lagrangian of order k . The standard power counting of χ EFT is recovered with the extended-on-mass-shell (EOMS) scheme [41], whereby the divergent parts of loop diagrams, along with the power-counting-breaking terms, are absorbed into the low-energy constants following the \overline{MS} prescription.

The set of $\mathcal{O}(\epsilon^3)$ χ EFT diagrams contributing to the spectral functions of the form factors on the two-pion cut at $t > 4M_\pi^2$ is shown in Fig. 4.² These are the loop diagrams in which

²To clarify the parametric counting, we note that $\mathcal{O}(\epsilon^3)$ refers to the order of the baryon electromagnetic vertex function, in which the background field is counted as $\mathcal{O}(\epsilon)$. The actual order of the spectral function extracted in this way is therefore $\mathcal{O}(\epsilon^2)$. Following standard usage we refer to our calculation as $\mathcal{O}(\epsilon^3)$, keeping in mind this distinction.

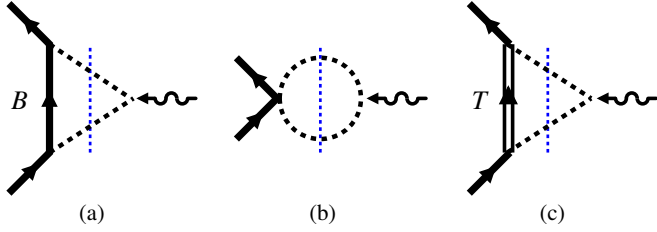


Figure 4: $O(\epsilon^3)$ χ EFT diagrams contributing to the spectral functions of the octet baryon isovector form factors on the two-pion (and two-kaon) cut. Dashed lines: pions (kaons); solid lines: octet baryons; double lines: decuplet baryons; wavy lines: electromagnetic field. The two-pion (or two-kaon) cut is indicated by the dotted blue line. Diagrams in which the electromagnetic field couples to the baryon or the meson-baryon vertices do not contribute to the two-pion (or two-kaon) cut and are not shown here.

the electromagnetic field couples to the baryon through two-pion exchange in the t -channel: the “triangle” diagrams (a) and (c) with octet and decuplet intermediate states, and the “tadpole” diagram (b). Within the dispersive representation Eq. (7) these diagrams account for the densities at peripheral distances $b = O(M_\pi^{-1})$. The two-kaon cut of the form factor at $t > 4M_K^2$, which results from the corresponding two-kaon exchange diagrams in Fig. 4, contributes only to the densities at much shorter distances $b = O(M_K^{-1})$ and can be neglected in the periphery (see below). The χ EFT diagrams in which the electromagnetic field couples to the baryon or the meson-baryon vertices (not shown in Fig. 4) have cuts only at $t > 4m_{B,T}^2$, or no cuts at all (polynomials); their contributions modify the densities only at distances $b = O(M_{B,T}^{-1})$ or through delta functions at $b = 0$ and can be neglected in the periphery.

For reference we list here the Lagrangians generating the propagators and vertices in the $O(\epsilon^3)$ diagrams of Fig. 4. The lowest-order Lagrangian for the interaction between octet mesons and the electromagnetic field is

$$\mathcal{L}_{\phi\phi}^{(2)} = \frac{f_0^2}{4} \text{Tr}(u_\mu u^\mu + \chi_+), \quad (20)$$

where the vielbein is given by $u_\mu = i\{u^\dagger, \nabla_\mu u\}$, $u^2 = U = \exp(i\sqrt{2}\phi/f_0)$, $\nabla_\mu u = \partial_\mu u - i(v_\mu + a_\mu)u + iu(v_\mu - a_\mu)u$; and the mass term is given by $\chi_+ = \chi U^\dagger + U\chi^\dagger$ with $\chi = 2B_0 \text{diag}(m_u, m_d, m_s)$, where m_f ($f = u, d, s$) are the quark masses; and f_0 is the meson decay constant in the chiral limit. For the couplings with the octet baryons we need the leading-order $SU(3)$ meson-baryon Lagrangian

$$\begin{aligned} \mathcal{L}_{B\phi}^{(1)} = & \text{Tr}(\bar{B}(i\mathcal{D} - m_{B0})B) + \frac{D}{2} \text{Tr}(\bar{B}\gamma^\mu\gamma_5\{u_\mu, B\}) \\ & + \frac{F}{2} \text{Tr}(\bar{B}\gamma^\mu\gamma_5[u_\mu, B]), \end{aligned} \quad (21)$$

where the covariant derivative acts as $\mathcal{D}_\mu B = \partial_\mu B + [\Gamma_\mu, B]$, with the chiral connection given by $\Gamma_\mu = \frac{1}{2}[u^\dagger, \partial_\mu u] - \frac{i}{2}u^\dagger(v_\mu + a_\mu)u - \frac{i}{2}u(v_\mu - a_\mu)u^\dagger$. The axial-vector fields a_μ are set to zero in our case, and the two axial couplings are fixed as $D = 0.80$ and $F = 0.46$ [51]. Finally, when introducing the decuplet baryons, the Lagrangians that are needed are

$$\mathcal{L}_{T\phi}^{(1)} = \bar{T}_\mu^{abc} (i\gamma^{\mu\nu\alpha} \mathcal{D}_\alpha - m_{T0}\gamma^{\mu\nu}) T_\nu^{abc}, \quad (22)$$

$$\mathcal{L}_{TB\phi}^{(1)} = \frac{iC}{m_{T0}} \epsilon^{ilm} [(\partial_\mu \bar{T}_\nu^{ijk}) \gamma^{\mu\nu\rho} u_\rho^{jl} B^{km} + \text{H.c.}], \quad (23)$$

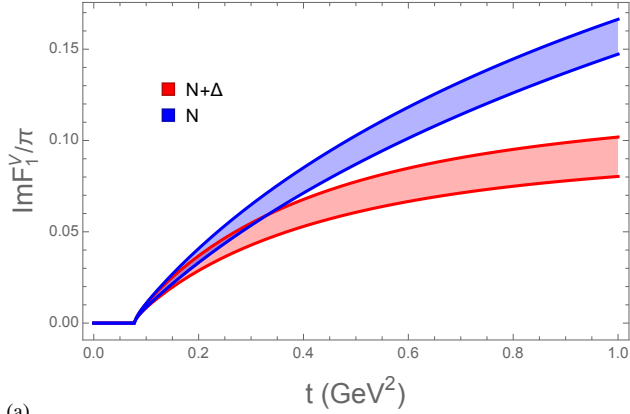
where $C = -h_A/(2\sqrt{2})$ is the octet-decuplet axial coupling, $\gamma^{\mu\nu} = \frac{1}{2}[\gamma^\mu, \gamma^\nu]$, $\gamma^{\mu\nu\rho} = \frac{1}{2}(\gamma^\mu\gamma^\nu\gamma^\rho - \gamma^\rho\gamma^\nu\gamma^\mu)$, and $\gamma^{\mu\nu\rho\sigma} = \frac{1}{2}[\gamma^{\mu\nu\rho}, \gamma^\sigma]$. The covariant derivative acts on the decuplet as $\mathcal{D}_\alpha T_\nu^{abc} = \partial_\alpha T_\nu^{abc} + (\Gamma_\alpha, T_\nu)^{abc}$, where $(X, Y)^{abc} = X^{ad}Y^{dbc} + X^{bd}Y^{adc} + X^{cd}Y^{abd}$. The vertices in Eqs. (22) and (23) are consistent vertices (they transform covariantly under point transformations), which effectively implement the projection on spin-3/2 degrees of freedom.

The spectral functions (imaginary parts) resulting from the t -channel cut of the diagrams of Fig. 4 can be obtained by applying cutting rules [18] and are given by finite phase-space integrals, which do not require renormalization. We have also calculated the form factors themselves from the full set of $O(\epsilon^3)$ diagrams for the baryon electromagnetic vertex function (not shown in Fig. 4), including loop diagrams and their renormalization, and verified electromagnetic gauge invariance of the result. We have confirmed that our expressions reproduce the ones of Ref. [47] when reduced to the $SU(2)$ flavor group. Further tests validating our calculation are described in Appendix A.

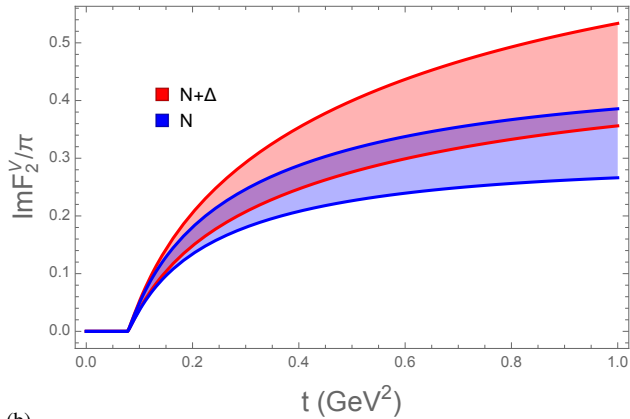
For the numerical evaluation we consider a range of values for the couplings and baryon masses that goes from the $SU(2)$ values ($m_B = 939$ MeV, $m_T = 1232$ MeV and $f_\pi = 92.2$ MeV, $h_A = 2.85$; see Ref. [47]) to the $SU(3)$ average values ($\bar{m}_B = 1151$ MeV, $\bar{m}_T = 1382$ MeV, $\bar{f}_\phi = 1.17f_\pi$, $h_A = 2.40$; see Refs. [49, 51]). This provides an uncertainty band associated with the systematic errors and gives an estimate of the expected higher-order corrections. The meson masses are taken at their physical values, $M_\pi = 139$ MeV, $M_K = 494$ MeV. According to the chiral expansion the meson mass differences are of the same order as the meson masses themselves, whereas the baryons have a common mass in the chiral limit and the mass splittings are suppressed. This circumstance has important consequences for the description of peripheral baryon structure, as it ensures that the pion and kaon exchange contributions to the densities are evaluated with the physical masses and possess the correct ranges $1/(2M_\pi)$ and $1/(2M_K)$ already in the lowest order.

The $O(\epsilon^3)$ χ EFT results for the nucleon isovector spectral functions are shown in Fig. 5. The steep rise above the threshold at $t = 4M_\pi^2$ is caused by the subthreshold singularity at $t = 4M_\pi^2 - M_\pi^4/m_N^2$ (on the unphysical sheet of the nucleon form factor), which results from the triangle diagram Fig. 4 (a) with an intermediate nucleon and is a general feature of the analytic structure. In the diagram (c) with intermediate Δ isobar the subthreshold singularity is further removed from threshold, resulting in a smaller contribution. The intermediate Δ contribution reduces the intermediate N result in the case of $\text{Im} F_1^V$, and enhances it in the case of $\text{Im} F_2^V$. We note that this pattern ensures the proper scaling behavior of the form factors in the large- N_c limit of QCD, where the N and Δ become degenerate [18, 26].

In Appendix B we compare the results of the present $O(\epsilon^3)$ calculation with those of Ref. [18, 26], which used an “incon-



(a)



(b)

Figure 5: $O(\epsilon^3)$ χ EFT results for the nucleon isovector spectral functions, with and without the intermediate $\Delta(1232)$ contribution, in the $SU(2)$ flavor limit.

sistent” form of the $\pi N \Delta$ vertex. The results for the Δ contribution agree at $O(\epsilon^3)$ but differ by higher-order terms, which cause numerical differences of 20% in $\text{Im } F_1$ (50% in $\text{Im } F_2$) at $t \sim 0.6 \text{ GeV}^2$ (see Fig. B.12).

3.2. Improvement through unitarity

The χ EFT expressions by themselves describe the baryon isovector spectral functions only in the near-threshold region $t = 4M_\pi^2 + \text{few } M_\pi^2$. This can be seen clearly in the case of the nucleon, where the χ EFT expressions can be compared with the spectral functions obtained from dispersion theory (see below) and was noticed in earlier χ EFT calculations [27, 28, 29, 30, 31]. The reason for the discrepancy is the strong rescattering within the $I = J = 1$ $\pi\pi$ system in the t -channel, which manifests itself in the ρ meson resonance at $t \sim 30M_\pi^2 = 0.6 \text{ GeV}^2$. In order to construct the baryon densities down to distances $b \sim 1 \text{ fm}$ we need to extend the calculation of isovector spectral functions into the ρ meson mass region (see Sec. 2.2 and Fig. 3). This can be accomplished in an approach that combines the χ EFT calculations with dispersion theory. We describe this approach first for the baryon form factors in which the two-pion cut starts at the normal threshold $t_{\text{thr}} = 4M_\pi^2$ (such as the nucleon $B = N$); the role of anomalous

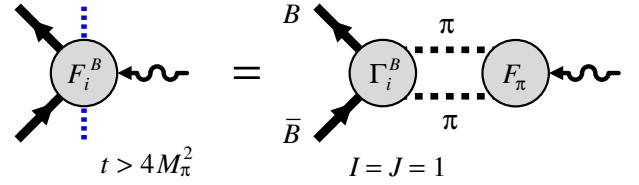


Figure 6: Unitarity relation for the isovector spectral function on the two-pion cut, Eq. (24).

thresholds with $t_{\text{thr}} < 4M_\pi^2$ in the strange baryon form factors will be considered subsequently.

On general grounds the baryon isovector spectral function on the two-pion cut can be expressed as (here t is real and $t > 4M_\pi^2$) [32, 33, 34]

$$\text{Im} F_i^B(t) = \frac{k_{\text{cm}}^3}{\sqrt{t}} \Gamma_i^B(t) F_\pi^*(t) \quad (i = 1, 2), \quad (24)$$

where $k_{\text{cm}} = \sqrt{t/4 - M_\pi^2}$ is the center-of-mass momentum of the $\pi\pi$ system in the t -channel, $\Gamma_i^B(t)$ is the complex $I = J = 1$ $\pi\pi \rightarrow B\bar{B}$ partial wave amplitude, and $F_\pi(t)$ is the complex pion form factor in the timelike region (see Fig. 6). Equation (24) follows from the unitarity condition in the t -channel and is valid strictly in the region up to the four-pion threshold, $4M_\pi^2 < t < 16M_\pi^2$; if contributions from four-pion states are neglected it can effectively be applied up to $t \sim 50M_\pi^2 = 1 \text{ GeV}^2$. The expression on the right-hand side of Eq. (24) is real because the complex functions $\Gamma_i^B(t)$ and $F_\pi(t)$ have the same phase on the two-pion cut (Watson theorem [53]). It is convenient to rewrite Eq. (24) in the form

$$\text{Im} F_i^B(t) = \frac{k_{\text{cm}}^3}{\sqrt{t}} \frac{\Gamma_i^B(t)}{F_\pi(t)} |F_\pi(t)|^2 \quad (i = 1, 2). \quad (25)$$

This representation has two advantages: (a) The function $\Gamma_i^B(t)/F_\pi(t)$ is real at $t > 4M_\pi^2$ and therefore has no two-pion cut; (b) the squared modulus $|F_\pi(t)|^2$ can be extracted directly from the $e^+e^- \rightarrow \pi^+\pi^-$ exclusive annihilation cross section, without determining the phase of the complex form factor. Equation (25) is a variant of the N/D method of amplitude analysis [55]. The $\pi\pi \rightarrow B\bar{B}$ t -channel partial-wave amplitude is represented in the form $\Gamma_i^B(t) = N(t)/D(t)$, such that the right-hand cut (related to the t -channel exchanges) appears only in the factor $1/D(t)$ and the left-hand cut (related to the s -channel intermediate states) in the factor $N(t)$. In the case at hand the D function is naturally chosen as the inverse pion form factor, $D(t) = 1/F_\pi(t)$ [34].

The representation Eq. (25) suggests a new approach to calculating the spectral function on the two-pion cut. We use χ EFT to calculate the real function $\Gamma_i^B(t)/F_\pi(t)$ at $t > 4M_\pi^2$ to a fixed order. We then multiply the result with the empirical $|F_\pi(t)|^2$, which contains the effects of $\pi\pi$ rescattering and the ρ meson resonance. The major advantage of this approach is that the χ EFT calculation is not affected by the strong $\pi\pi$ rescattering, which would require higher-order unitarity corrections when

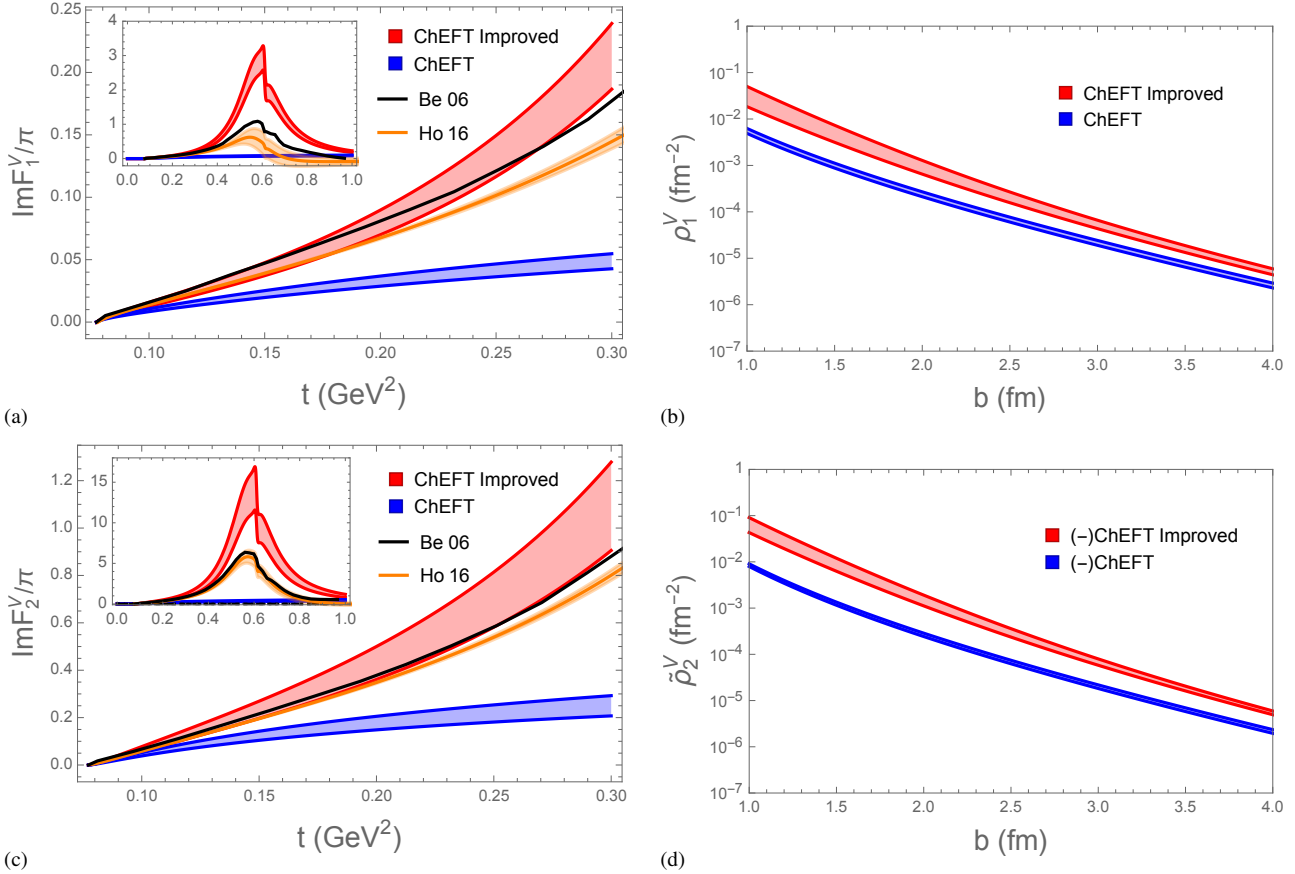


Figure 7: (a), (c) Nucleon isovector spectral functions obtained from $\mathcal{O}(\epsilon^3)$ χ EFT and the improvement through unitarity, Eq. (26). Blue bands: $\mathcal{O}(\epsilon^3)$ χ EFT results, including contributions from both N and Δ intermediate states, cf. Fig. 5. Red bands: Results after improvement through unitarity, Eq. (26). Brown bands and black line: Spectral functions obtained from Roy-Steiner equations [36] and analytic continuation of the $\pi\pi \rightarrow N\bar{N}$ amplitudes [35, 37]. The main plot shows the functions up to $t = 0.3 \text{ GeV}^2$; the inset shows them up to $t = 1 \text{ GeV}^2$. (b), (d) Effect of improvement on the peripheral transverse densities. The isovector magnetic density is shown with opposite sign ($-$) on the logarithmic scale.

treated within the χ EFT. We therefore expect this approach to show much better convergence than direct χ EFT calculations of the spectral function. From a general perspective, the organization according to Eq. (25) is consistent with the idea of separation of scales basic to χ EFT. The function $\Gamma_i^B(t)/F_\pi(t)$ is dominated by the singularities of the baryon Born diagrams (or diagrams with πB inelastic intermediate states in higher orders), which are governed by the scales M_π and $m_T - m_B$ (the octet-decuplet mass difference). The t -dependence of the pion form factor, in contrast, is governed by the chiral-symmetry-breaking scale Λ_χ , which is of the order of the vector meson mass.

In our χ EFT calculation of the spectral function at $\mathcal{O}(\epsilon^3)$ in Sec. 3.1 the function $\Gamma_i^B(t)/F_\pi(t)$ is effectively evaluated at $\mathcal{O}(\epsilon^0)$ (cf. Footnote 2). At this level the pion form factor in the denominator enters at leading order, $F_\pi(t) \equiv 1$, so that the χ EFT result for $\Gamma_i^B(t)/F_\pi(t)$ is the same as that for $\Gamma_i^B(t)$ itself. The prescription of Eq. (25) therefore simply amounts to multiplying our $\mathcal{O}(\epsilon^3)$ results for the spectral functions by $|F_\pi(t)|^2$,

$$\text{Im}F_i^B(t) [\text{improved}] = \text{Im}F_i^B(t) [\chi\text{EFT}] \times |F_\pi(t)|^2$$

$$(i = 1, 2). \quad (26)$$

This formula permits an extremely simple implementation of unitarity at $\mathcal{O}(\epsilon^3)$. For the pion form factor we use the Gounaris-Sakurai parametrization including effects of ρ - ω mixing [70, 71], with the parameters determined in Ref. [39]. The prescription Eq. (26) results in a remarkable improvement of the χ EFT predictions for the spectral functions. The improved χ EFT results for the nucleon ($B = N$) reproduce the spectral functions obtained from amplitude analysis (analytic continuation of the $\pi\pi \rightarrow N\bar{N}$ partial-wave amplitudes [35, 37], Roy-Steiner equations [36]) up to $t \sim 16 M_\pi^2 = 0.3 \text{ GeV}^2$ within errors (see Fig. 7a and c). Note that this is achieved without adding any free parameters and represents a genuine prediction of χ EFT. The improved $\mathcal{O}(\epsilon^3)$ results have qualitatively correct behavior even in the ρ meson mass region. We expect that higher-order χ EFT corrections to the ratio $\Gamma_i^B(t)/F_\pi(t)$ would further improve the agreement with the dispersion-theoretical results at $t > 0.3 \text{ GeV}^2$ [54].

The improvement according to Eq. (26) has a dramatic effect on the peripheral transverse densities of the nucleon (see Fig. 7b and d). At distances $b \sim 1 \text{ fm}$ the improved predictions are up to

an order of magnitude larger than what would be obtained with the original χ EFT results. At distances $b \sim 3$ fm the change is still by a factor ~ 3 . At asymptotically large distances (much larger than those shown in the figure) the improvement would change the densities by the constant factor $|F_\pi(t = 4M_\pi^2)|^2 \approx 1.3$.

In order to extend the dispersive improvement to the other octet baryons it is necessary to discuss the role of anomalous thresholds in the strange baryon form factors [72, 73]. In the normal situation considered so far, the Born terms in the $\pi\pi \rightarrow B\bar{B}$ amplitudes give rise to singularities on the unphysical sheet of the baryon form factor, and the principal cut starts at the normal threshold $t_{\text{thr}} = 4M_\pi^2$. Such is the case with the N and Δ Born terms in the $\pi\pi \rightarrow N\bar{N}$ amplitudes. In certain special situations the Born term singularities in the $\pi\pi \rightarrow B\bar{B}$ amplitudes move onto the physical sheet of the form factor and give rise to cuts with anomalous thresholds at $t_{\text{thr}} < 4M_\pi^2$. This occurs if [72]

$$m_B^2 > m_{B'}^2 + M_\pi^2, \quad (27)$$

where $m_{B'}$ is the mass of the baryon pole in the Born term, and the anomalous threshold is located at

$$t_{\text{thr}} = 4M_\pi^2 - (m_B^2 - m_{B'}^2 - M_\pi^2)^2/m_{B'}^2 < 4M_\pi^2. \quad (28)$$

Such is the case for the Λ pole in the $\pi\pi \rightarrow \Sigma\bar{\Sigma}$ amplitudes, which produces an anomalous threshold at $t_{\text{thr}} = 3.08 M_\pi^2$. In a general dispersion-theoretical treatment with exact masses the contribution from the anomalous cut would need to be considered explicitly in the spectral representation of the form factors and the densities. In the present treatment based on leading-order χ EFT anomalous thresholds do not occur, as the octet baryon masses are taken at a common value in the chiral limit (this is required by the small-scale expansion) and therefore $m_{B'} = m_B$ in Eq. (27). We can thus use Eq. (26) at leading order for the entire baryon octet. This feature is a consequence of our particular combination of χ EFT and dispersion theory and permits a major simplification of the description of the strange baryon form factors. The anomalous threshold in the Σ form factors appears only in higher-order χ EFT calculations and affects the behavior of the densities at very large distances; its contribution at realistic distances $b \sim 1 - 4$ fm is expected to be small (cf. the discussion in Sec. 2.2 and Fig. 3).

An anomalous threshold would also appear in the $K\bar{K} \rightarrow \Sigma\bar{\Sigma}$ amplitudes through the N Born term, at $t_{\text{thr}} = 4M_K^2 - (m_\Sigma^2 - m_N^2 - M_K^2)^2/m_N^2 = 3.6 M_K^2 < 4M_K^2$, cf. Eq. (28), if the exact baryon masses were used. Again this feature is absent in our leading-order χ EFT calculation, where the N and Σ are taken at a common mass. In any case this anomalous threshold is only marginally lower than the normal $K\bar{K}$ threshold, so that its cut corresponds to a high-mass contribution that can be neglected in the peripheral densities on the same grounds as the normal $K\bar{K}$ cut.

Based on the preceding considerations we now use the prescription Eq. (26) to calculate the isovector spectral functions of the strange octet baryons on the two-pion cut. While we cannot compare with a dispersion-theoretical result in this case, we expect the approximation to be of similar quality as in the case

	N		Σ		Ξ		$\Lambda - \Sigma$	
	8	10	8	10	8	10	8	10
$\text{Im } F_1^V$	+	-	+	+	+	+	-	-
$\text{Im } F_2^V$	+	+	+	-	+	-	-	+

Table 1: Signs of intermediate octet and decuplet contributions to the isovector spectral functions of the octet baryon form factors, $\text{Im } F_i^V$ ($i = 1, 2$) on the two-pion cut.

of the nucleon. The results for $\text{Im } F_1^V$ and $\text{Im } F_2^V$ are shown in Fig. 8 [see Eq. (13) for the definition of the isovector component in the octet baryon states]. They exhibit several interesting features. (a) In the near-threshold region $t = 4M_\pi^2 + \text{few } M_\pi^2$ (see Fig. 8a, c) the dominant contribution to the spectral functions comes from the triangle diagram with intermediate octet baryons, Fig. 4a. The ratios of the spectral functions for the different baryons are therefore determined approximately by the ratios of the products of the $B \rightarrow B'\pi$ couplings for the relevant intermediate states, which follow directly from the $SU(3)$ chiral Lagrangian Eq. (21):

$$\begin{aligned} \text{Im } F_1^{N,V} &: \quad \text{Im } F_1^{\Sigma,V} &: \quad \text{Im } F_1^{\Xi,V} &: \quad \text{Im } F_1^{\Lambda-\Sigma,V} \\ &= (F + D)^2 &: \quad (2F^2 + \frac{2}{3}D^2) &: \quad (F - D)^2 &: \quad (-\frac{2}{\sqrt{3}}FD) \\ &= 1.59 &: \quad 0.85 &: \quad 0.12 &: \quad (-0.42) \end{aligned} \quad (29)$$

(b) At larger values of t (see Fig. 8b, d) the spectral functions receive sizable contributions from the triangle diagram with intermediate decuplet baryons and the contact terms, Fig. 4c and b. These contributions change the relative order of the different baryons compared to the near-threshold region dominated by intermediate octet baryons. The signs of the intermediate octet and decuplet contributions are summarized in Table 1. In the Dirac form factor the intermediate decuplet contributes to $\text{Im } F_1^{N,V}$ with *opposite* sign to the intermediate octet, and to $\text{Im } F_1^{\Sigma,V}$ and $\text{Im } F_1^{\Xi,V}$ with the *same* sign. As a result, $\text{Im } F_1^{\Sigma,V}$ is now larger than $\text{Im } F_1^{N,V}$, and $\text{Im } F_1^{\Xi,V}$ is comparable to $\text{Im } F_1^{N,V}$. In the Pauli form factor the intermediate decuplet contributes to $\text{Im } F_2^{N,V}$ with the *same* sign as the intermediate octet, and to $\text{Im } F_2^{\Sigma,V}$ and $\text{Im } F_2^{\Xi,V}$ with *different* sign. As a result the relative order of $\text{Im } F_2^{N,V}$ and $\text{Im } F_2^{\Sigma,V}$ remains the same, while $\text{Im } F_2^{\Xi,V}$ becomes negative at larger values of t . These changes between the near-threshold region and larger values of t are a non-trivial consequence of the inclusion of decuplet degrees of freedom in the χ EFT.

To complete our assessment we want to quantify also the contribution of the two-kaon cut to the peripheral isovector densities in χ EFT. Numerical evaluation shows that in the nucleon at $b = 1$ fm the isovector density from the two-kaon cut is smaller than that from the two-pion cut by an order of magnitude; at $b = 2$ fm it is already smaller by two orders of magnitude. Similar ratios are obtained for the strange octet baryons. We can therefore neglect the contributions of the two-kaon cut in the peripheral isovector densities. The quoted kaon/pion ratios refer to the χ EFT densities before the dispersive improvement. An

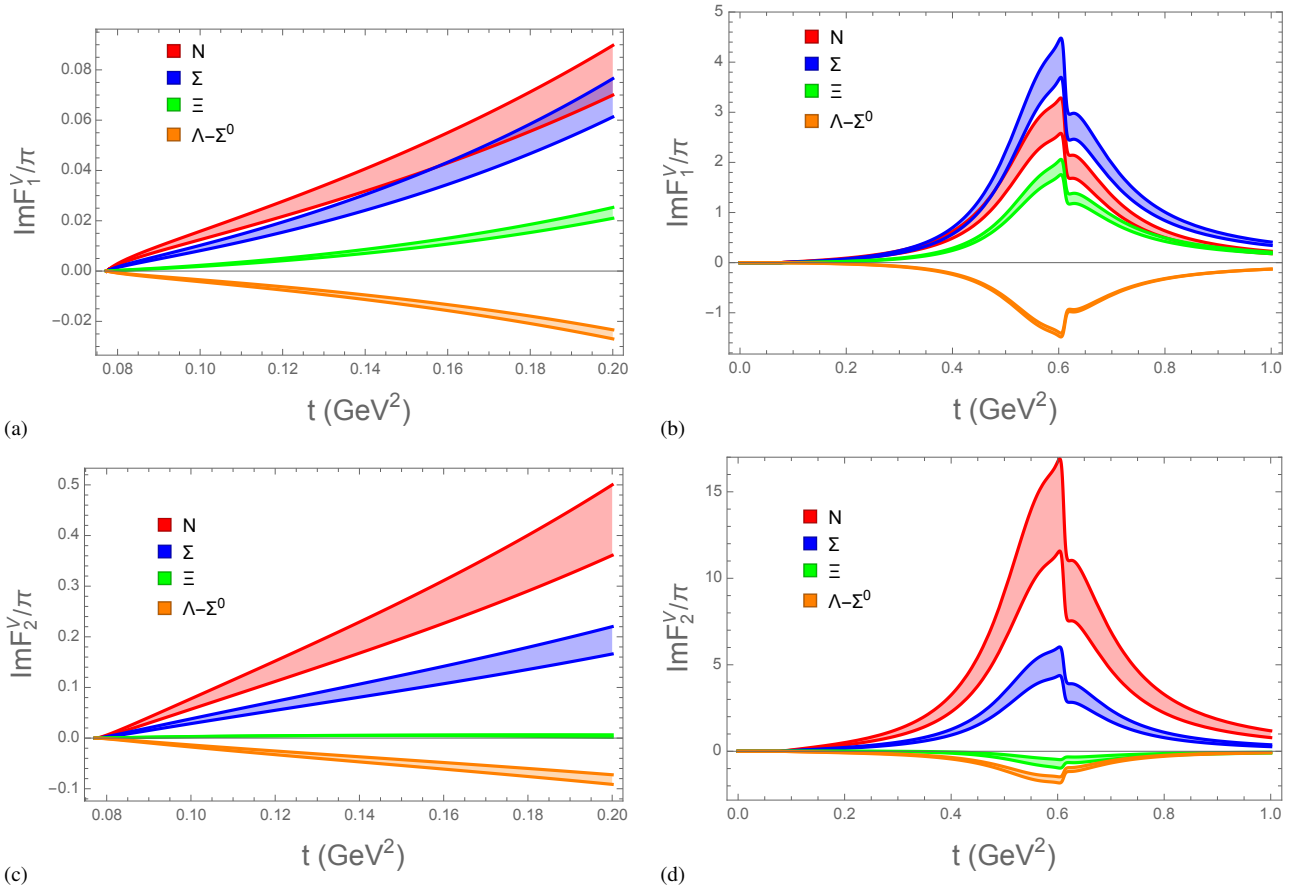


Figure 8: Isovector component of the spectral functions of the octet baryons, cf. Eq. (13), as obtained from $\mathcal{O}(\epsilon^3)$ χ EFT with dispersive improvement, Eq. (26). (a), (b) Dirac form factors F_1^V . (c), (d) Pauli form factors F_2^V . Plots (a), (c) show the near-threshold region; plots (b), (d) show the region up to $t = 1$ GeV 2 .

interesting theoretical question is how the dispersive improvement could be extended to the kaon sector through a coupled-channel formalism.

3.3. Isoscalar spectral functions

The isoscalar component of the baryon spectral functions behaves very differently from the isovector one and requires separate treatment. In the limit of exact isospin symmetry the isoscalar spectral functions arise from the exchange of an odd number of pions in the t -channel (G-parity). The lowest-mass exchange with vector quantum numbers is the three-pion exchange ($t > 9 M_\pi^2$). In χ EFT this contribution appears only at $\mathcal{O}(\epsilon^7)$ and is very small [28]. Inclusion of the ω resonance through unitarity in the three-pion channel, in analogy to our treatment of the ρ in the two-pion channel, would be possible in principle but requires three-body unitarity techniques that are not readily available.

The present $SU(3)$ -flavor χ EFT generates an isoscalar term in the spectral function through two-kaon exchange. Its contribution to the peripheral densities is extremely small compared to the isovector densities, or the isoscalar densities resulting from ω and ϕ exchange (see below). Treatment of the ϕ as a resonance in the two-kaon channel, along the lines of the ρ in

the two-pion channel, is impractical because of the mixing with the three-pion and other hadronic channels; see Refs. [74, 75] for a discussion.

In the present study we therefore model the isoscalar spectral functions of the octet baryons at $t < 1$ GeV 2 through phenomenological vector meson exchange (ω, ϕ),

$$\text{Im} F_i^{B,S}(t) = \pi \sum_{V=\omega,\phi} a_i^{VBB} \delta(t - M_V^2) \quad (i = 1, 2). \quad (30)$$

The vector meson couplings of the octet baryons are obtained from $SU(3)$ symmetry, certain assumptions about the F/D ratio, and the empirical vector meson couplings to the nucleon; see Appendix C. The contribution from states with $t > 1$ GeV 2 is strongly suppressed in the peripheral densities, so that the two-pole parametrization Eq. (30) is sufficient for our purposes. We do not aim for a precise description of the isoscalar sector here, as the peripheral densities are dominated by the isovector component.

4. Octet baryon densities

4.1. Charge and magnetization densities

Using the spectral functions calculated in Sec. 3 we now calculate the peripheral transverse densities of the octet baryons

and study their properties. The studies of Sec. 2.2 have shown that at distances $b > 1$ fm the dispersion integrals Eqs. (8) and (9) are dominated by masses $t < 1$ GeV², where our approximations in the spectral functions are justified.

In order to quantify the uncertainties of the peripheral densities we propagate the estimated theoretical uncertainties of the spectral functions through the dispersion integrals Eqs. (8) and (9). In the isovector spectral functions we use the estimated χ EFT errors in the region $t < 16M_\pi^2$ (as shown by the error bands in Fig. 7a and c) and assign an additional error of $\pm 50\%$ in the ρ meson mass region (these error bands are not shown in the insets of Fig. 7a and c but inferred from the comparison of the improved χ EFT results with the amplitude analysis results [35, 36] in this region). In the isoscalar spectral functions we generate an error band from the uncertainties of the empirical ωNN couplings extracted from fits to the isoscalar nucleon form factor data [38] (see Appendix C and the parameters in Table C.3). Note that the error estimates performed here are specific to the peripheral densities and do not take into account constraints resulting from the total isovector/isoscalar charges of the baryons, which would involve the densities at central as well as peripheral distances; these constraints would significantly reduce the error of the overall densities at $b \sim 1$ fm.

The resulting charge densities $\rho_1^B(b)$ and magnetization densities $\bar{\rho}_2^B(b)$ are summarized in Figs. 9 and 10. For each octet baryon B we show the total densities as well as their isovector and isoscalar components, defined according to Eq. (13),

$$\left. \begin{aligned} \{\rho^p, \rho^n\} &= \rho^{N,S} \pm \rho^{N,V}, \\ \rho^\Lambda &= \rho^{\Lambda,S}, \\ \{\rho^{\Sigma^+}, \rho^{\Sigma^-}\} &= \rho^{\Sigma,S} \pm \rho^{\Sigma,V}, \\ \rho^{\Sigma^0} &= \rho^{\Sigma,S}, \\ \rho^{\Lambda-\Sigma} &= \rho^{\Lambda-\Sigma,V}, \\ \{\rho^{\Xi^0}, \rho^{\Xi^-}\} &= \rho^{\Xi,S} \pm \rho^{\Xi,V}. \end{aligned} \right\} \quad (31)$$

The densities with definite sign (positive or negative) are plotted on a logarithmic scale; for the densities with changing sign the plots show the radial densities $2\pi b\rho_1(b)$ and $2\pi b\bar{\rho}_2(b)$ on a linear scale. Several general features of the results are worth noting: (a) The densities decay exponentially at large b , as dictated by the analytic properties of Eqs. (8) and (9). The decay rate depends on the effective masses in the spectral integral. The isovector densities decay approximately as $\sim \exp(-M_\rho b)$ at $b \sim 1$ fm, and with a smaller effective mass at $b > 2$ fm, reflecting the changing distribution of strength in the spectral integrals (see Fig. 3).³ The isoscalar densities decay as $\exp(-M_\omega b)$ at all $b > 1$ fm. (b) At distances $b > 3$ fm the overall densities are dominated by the isovector component (if present). Isoscalar and isovector densities become comparable only at distances $b < 2$ fm. (c) Our approximations allow us to reconstruct the isovector density with an uncertainty of $\sim \pm 30\%$ at $b = 2$ fm, and with significantly lower uncertainty at larger distances. We

³A decay of the isovector densities as $\sim \exp(-2M_\pi b)$ is observed only at extremely large distances $b \sim m_N^2/M_\pi^2$, where the dispersive integrals are dominated by the extreme near-threshold region $t - 4M_\pi^2 \sim M_\pi^2/m_N^2$; see Ref. [18] for discussion.

now want to inspect the densities of the individual baryon multiplets.

Proton and Neutron. The nucleon isovector densities were studied in χ EFT in Ref. [18]. The dispersive improvement of the χ EFT spectral functions carried out in the present work (see Sec. 3.2) significantly increases the peripheral densities (see Fig. 8b and d) and allows us to construct them down to much smaller distances $b \gtrsim 1$ fm. The nucleon isovector and isoscalar charge densities are both positive (see Fig. 9). In the proton charge density the isovector and isoscalar contribute with the same sign, leading to a positive total density with smooth behavior. In the neutron charge density the isovector and isoscalar contribute with opposite sign, causing cancellations and varying behavior of the total density. At distances $b > 2$ fm the isovector dominates and the total neutron charge density is negative, as expected from the intuitive picture of the ‘‘pion cloud’’ resulting from $n \rightarrow \pi^- + p$ transitions (this interpretation can be demonstrated rigorously in the light-front representation of chiral dynamics [24, 25, 26]). At shorter distances $b \sim 1$ fm our results are consistent with a positive charge density in the neutron, as is observed in the empirical densities and has been discussed in the literature [8, 40]; however, the uncertainties of our present calculation are large and do not allow us to predict the sign at $b < 2$ fm.

In the nucleon magnetization density the isoscalar component is significantly smaller than in the charge density, due to the comparatively small value of the ωNN tensor coupling (see Fig. 10). As a result, the isovector magnetization density dominates down to much smaller distances $b \sim 1$ fm, and the proton and neutron have approximately opposite magnetization densities in the periphery.

In Refs. [18, 24] it was observed that the peripheral isovector nucleon charge and magnetization densities satisfy an approximate inequality $|\bar{\rho}_2^N(b)| < \rho_1^N(b)$. It applies to the densities arising from the triangle diagrams with nucleon intermediate states and can be derived rigorously in the light-front representation of chiral dynamics [24, 25, 26]. The contributions from Δ intermediate states violate the inequality (in the large- N_c limit of QCD they restore the hierarchy $|\bar{\rho}_2^N(b)| \gg \rho_1^N(b)$ required by general scaling arguments). The results of the present calculation confirm these observations.

Λ and Σ^0 . In the Λ and Σ^0 charge and magnetization densities the isovector component is absent, cf. Eq. (31). In the χ EFT description this happens by way of cancellation of the π^+ and π^- contributions from the triangle diagrams with $\pi^\pm \Sigma^\mp$ intermediate states, and similarly for the diagrams with $\pi^\pm \Sigma^{*\mp}$ intermediate states. The Λ and Σ^0 densities are thus pure isoscalar. They are dominated by ω and ϕ exchange down to distances $b \sim 1$ fm and are an order of magnitude smaller than the densities of the other baryons at $b > 2$ fm. In our parametrization based on $SU(3)$ symmetry the vector couplings are the same for the Λ and Σ^0 , $a_1^{\omega\Lambda\Lambda} = a_1^{\omega\Sigma^0\Sigma^0}$ (and similarly for ϕ) (see Appendix C and Table C.2), resulting in identical peripheral charge densities (see Fig. 9). In contrast, the tensor couplings have opposite signs, $a_2^{\omega\Lambda\Lambda} \approx -a_2^{\omega\Sigma^0\Sigma^0}$, giving rise to approximately opposite magnetization densities (see Fig. 10).

Λ - Σ^0 transition. The Λ - Σ^0 transition densities are pure

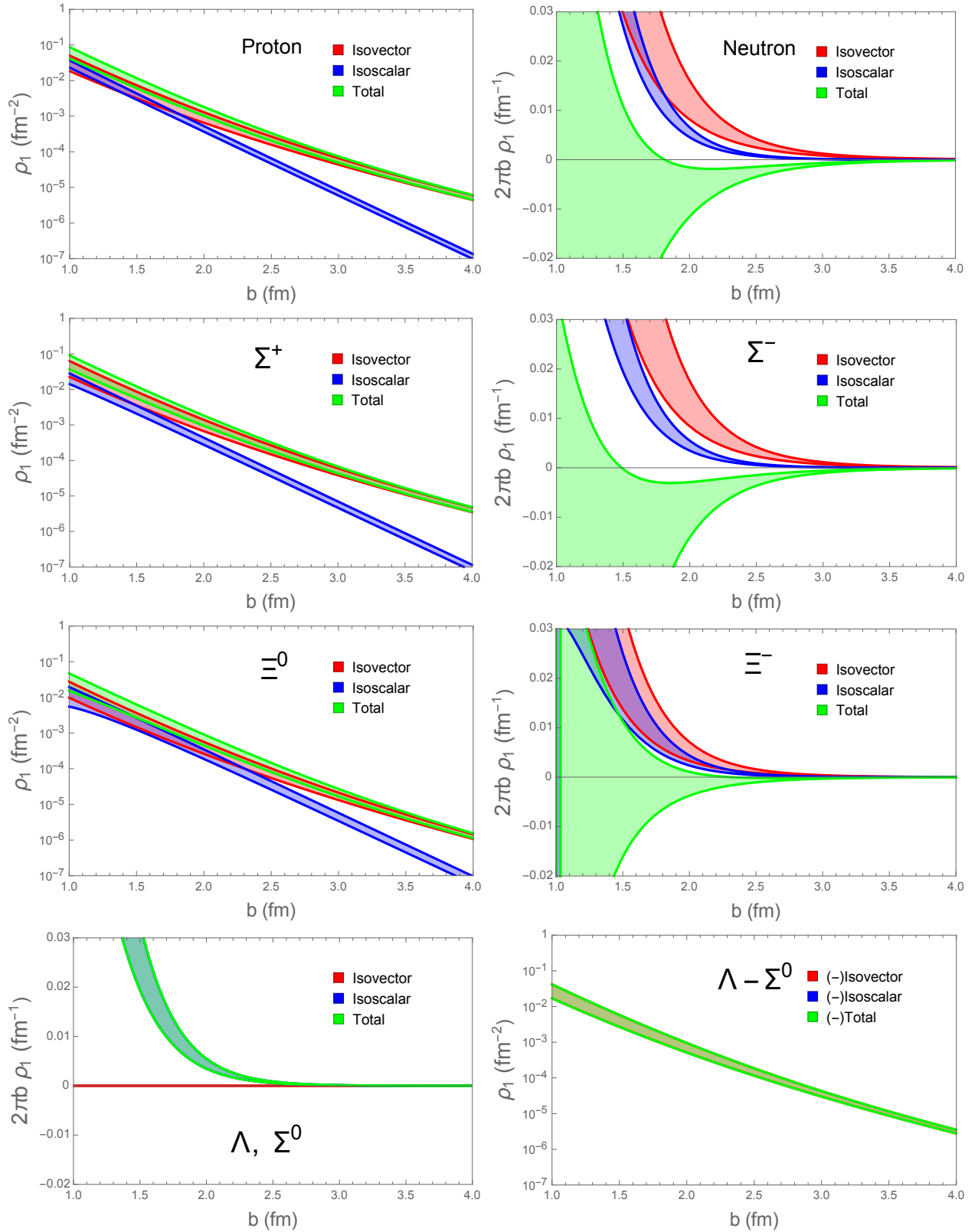


Figure 9: Transverse charge densities of the octet baryons. Red: Isovector component calculated using χ EFT and dispersive improvement. Blue: Isoscalar component estimated from vector meson poles. Green: Total density (sum or difference of isoscalar and isovector components). For the densities with fixed sign we plot $\rho_1(b)$ on a logarithmic scale (the signs are indicated in the legends of the plots); for those with changing sign we plot the radial densities $2\pi b \rho_1(b)$ on a linear scale.

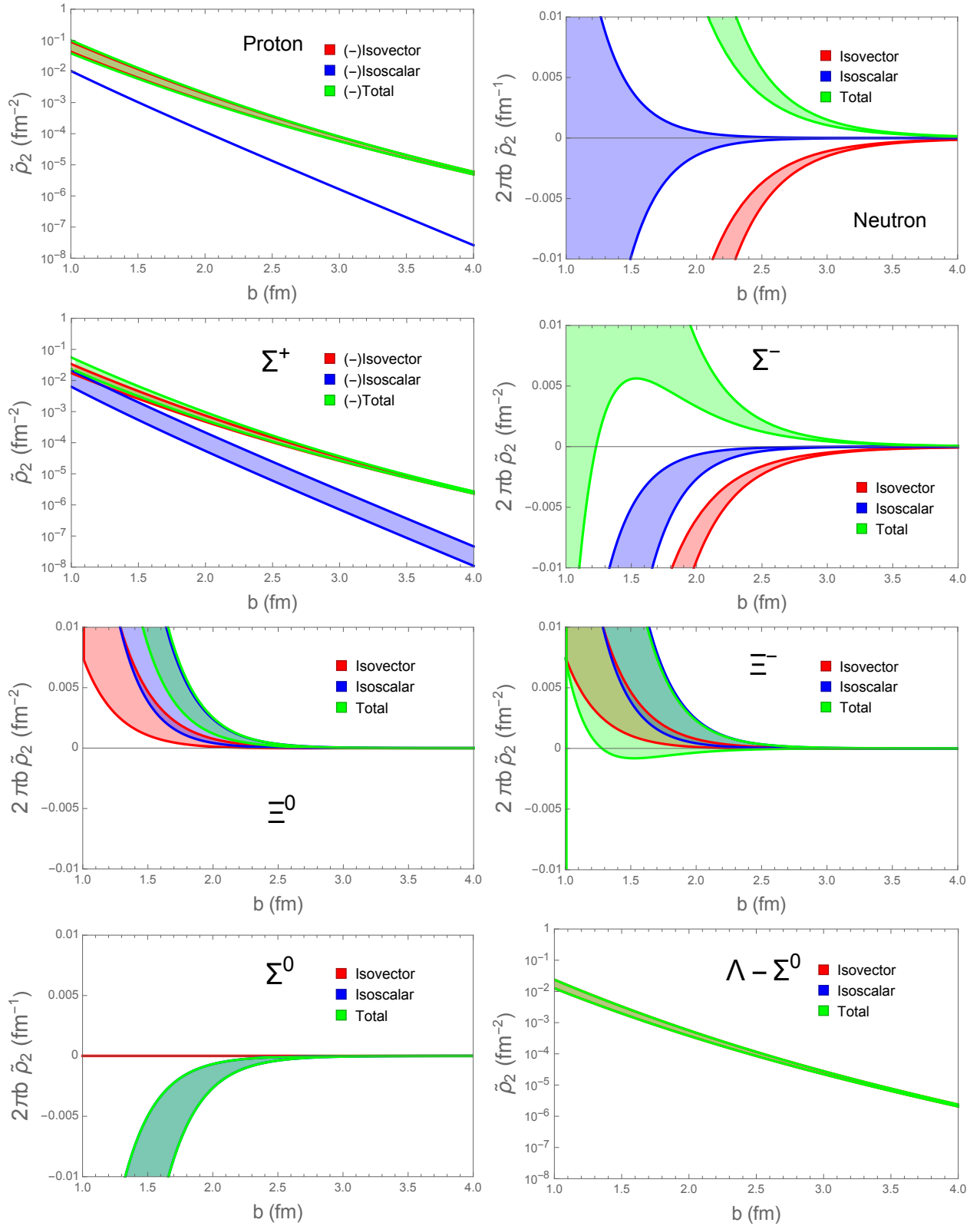


Figure 10: Transverse magnetization densities of the octet baryons. Red: Isovector component calculated using χ EFT and dispersive improvement. Blue: Isoscalar component estimated from vector meson poles. Green: Total density (sum or difference of isoscalar and isovector components). For the densities with fixed sign we plot $\tilde{\rho}_2(b)$ on a logarithmic scale (the signs are indicated in the legends of the plots); for those with changing sign we plot the radial densities $2\pi b \tilde{\rho}_2(b)$ on a linear scale.

isovector, cf. Eq. (31). They receive sizable peripheral contributions from the chiral processes with $\pi^\pm\Sigma^\mp$ (octet) and $\pi^\pm\Sigma^{*\mp}$ (decuplet) intermediate states. The signs of the transition charge and magnetization densities are opposite to those of the nucleon densities (see Figs. 9 and 10), as can be inferred already from the spectral functions (see Fig. 8). The relative magnitude of the isovector densities at distances $b \gtrsim 3$ fm is determined by the ratio of the spectral functions near threshold, cf. Eq. (29) and Fig. 8a and c; at distances $b \sim 1$ fm it is given by the ratio of the spectral functions in the vector meson mass region, cf. Fig. 8b and d.

Σ^+ and Σ^- . The charge densities of the Σ^+ and Σ^- baryons are similar to the ones in the proton and neutron (see Fig. 9). In difference to the Σ^0 , in the Σ^\pm densities both isovector and isoscalar components are present, cf. Eq. (31). The isovector charge densities $\rho^{\Sigma,V}$ and $\rho^{N,V}$ are similar at all distances $b > 1$ fm, because the isovector Σ spectral function is close to the nucleon one both near threshold and in the vector meson region, cf. Fig. 8a and b. The isoscalar charge densities $\rho^{\Sigma,S}$ and $\rho^{N,S}$ are likewise similar, because the ω couplings of the two baryons are close (see Table C.2). Altogether therefore the Σ^+ charge density is very close to that of the proton, and the Σ^- charge density shows a sign change similar to the neutron; the details depend on the accuracy of our calculation of the isovector spectral functions and the modeling of the isoscalar ones.

The Σ^+ and Σ^- magnetization densities are again similar to the ones in the proton and neutron, with some notable differences compared to the charge densities (see Fig. 10). In the magnetization densities the isovector $\tilde{\rho}_2^{\Sigma,V}$ is smaller than $\tilde{\rho}_2^{N,V}$ by about a factor $\sim 1/2$, while the isoscalar $\tilde{\rho}_2^{\Sigma,S}$ is larger in magnitude than $\tilde{\rho}_2^{N,S}$.

Ξ^0 and Ξ^- . In the Ξ baryons the peripheral isovector charge density is substantially smaller than in the nucleon or charged Σ states (see Fig. 9). This reflects the fact that the isovector spectral function of the Ξ is relatively suppressed near threshold, cf. Eq. (29) and Fig. 8 a and c, because the intermediate octet contribution to the Ξ is small and comparable to the decuplet one. (In the other baryons the octet intermediate states clearly dominates in the periphery.) At the same time, the isoscalar density of the Ξ has normal size. As a result, in the Ξ charge density the isoscalar and isovector become comparable at slightly larger distances than in the nucleon and Σ . This has interesting consequences for the charge density of the Ξ^- baryon, which is the difference of the isoscalar and isovector components. It suggests a sign change from a negative charge density at large b to a positive one at intermediate b , similar to the neutron, but with the transition happening at larger b than in the neutron (we cannot confirm this behavior as the estimated uncertainty of the total Ξ^- charge density is larger than that of the neutron in the present calculation).

The results for the Ξ magnetization density resemble those for the Σ^0 and Λ baryons (see Fig. 10). Although an isovector component is present in the Ξ spectral function, it is extremely small (see Fig. 8), resulting in a tiny contribution to the magnetic density, (see Fig. 10). On the other hand, the contribution of the isoscalar vector mesons is larger for the Ξ baryons than

for the rest of the baryons in the octet. This results in a magnetic density clearly dominated by the isoscalar component, even in the peripheral region. Given that the isoscalar component contributes in the same way for both, the Ξ^0 and Ξ^- , and that the isovector component is negligible, the magnetic density profile comes out almost exactly the same for both baryons.

4.2. Flavor decomposition

It is interesting to study the quark flavor decomposition of the transverse charge and magnetization densities in the octet baryons [40]. For each baryon B the densities can be decomposed as

$$\rho_i^B = e_u \rho^{B,u} + e_d \rho^{B,d} + e_s \rho^{B,s} \quad (i = 1, 2), \quad (32)$$

where $\rho_i^{B,f}(b)$ ($f = u, d, s$) represent the densities associated with the vector currents of the quark fields with flavor f , $J_f^\mu = \bar{\psi}_f \gamma^\mu \psi_f$; the quark charge factors are included explicitly in Eq. (32). The flavor densities $\rho_1^{B,f}$ satisfy the sum rules

$$\int d^2b \rho_1^{B,f}(b) = N_f, \quad (33)$$

where N_f represents the total quark flavor content of the baryon as determined by the isospin and hypercharge; i.e., the number of ‘‘valence quarks’’ in the baryon. In the context of GPDs the densities $\rho_1^{B,f}$ represent the integral of the quark and antiquark distributions at transverse distance b over the light-front momentum fraction x ,

$$\rho_1^{B,f}(b) = \int_0^1 dx [f^{B,f}(x, b) - f^{B,\bar{f}}(x, b)]. \quad (34)$$

The flavor densities $\rho_2^{B,f}$ are related in a similar manner to the quark distributions associated with the baryon helicity-flip GPDs. Note that the densities $\rho_1^{B,f}$ can be positive or negative, depending on whether there are more quarks or antiquarks of flavor f at a given transverse position b . The flavor densities within the isospin multiplets are related by isospin symmetry,

$$\left. \begin{aligned} \rho_i^{p,u} &= \rho_i^{n,d}, & \rho_i^{p,s} &= \rho_i^{n,s}, \\ \rho_i^{\Sigma^+,u} &= \rho_i^{\Sigma^-,d}, & \rho_i^{\Sigma^+,s} &= \rho_i^{\Sigma^-,s} = \rho_i^{\Sigma^0,s}, \\ \rho_i^{\Sigma^0,u} &= \rho_i^{\Sigma^0,d}, \\ \rho_i^{\Xi^0,u} &= \rho_i^{\Xi^0,d}, & \rho_i^{\Xi^0,s} &= \rho_i^{\Xi^0,s}. \end{aligned} \right\} \quad (35)$$

For the flavor decomposition of the form factors and densities we need to separate the contributions of non-strange (u, d) and strange (s) quarks in the isoscalar electromagnetic current [cf. Eq. (31)]

$$\rho_i^{B,S} = \rho_i^{B,u+d} + \rho_i^{B,s} \quad (i = 1, 2). \quad (36)$$

In our model of the isoscalar spectral functions, Eq. (30), the $u + d$ densities are identified with the contribution of the ω pole, while the s densities are identified with the ϕ pole. We emphasize that this identification is based on the assumptions of vector dominance and ideal mixing (see Appendix C) and can only provide a rough estimate of the strange-nonstrange separation

of the isoscalar current (for a discussion of the uncertainties of the flavor separation of the isoscalar nucleon form factors, see Refs. [74, 75, 76]). The results presented in the following are intended only to illustrate the basic features of the spatial dependence of the flavor densities in the peripheral region.

Using Eqs. (35) and (36) it is straightforward to calculate the quark flavor densities in terms of the baryon isovector, isoscalar up-down, and isoscalar strange densities. The quark flavor densities drop exponentially at large b with a rate determined by the relevant t -channel exchanges. In the u and d quark densities the isovector two-pion exchange dominates at large b (if present) and causes the densities to be of equal magnitude and opposite sign,

$$\rho_1^{B,u}(b) = -\rho_1^{B,d}(b) \quad (b \rightarrow \infty, B = p, n, \Sigma^\pm, \Xi^0, \Xi^-). \quad (37)$$

In the p, Σ^+ and Ξ^0 the peripheral u density is positive, and the d density is negative, as they result from processes with emission of a π^+ contributing to the u quark and d antiquark densities; in the n, Σ^- and Ξ^- the signs are opposite. At shorter distances $b < 2$ fm the u and d densities can show more complex behavior, as the isovector and isoscalar non-strange exchanges become comparable (ρ and ω). The strange quark density drops with the range of ϕ exchange and has no long-range component.

Of particular interest for baryon structure is the relative contribution of the various quark flavors to the charge density in the baryon at a given distance. It is convenient to consider the ratios

$$R^{B,f}(b) \equiv \frac{e_f \rho_1^{B,f}(b)}{\sum_{f'} e_{f'} \rho_1^{B,f'}(b)} = \frac{e_f \rho_1^{B,f}(b)}{\rho_1^B(b)}, \quad (38)$$

which at any b satisfy

$$\sum_f R^{B,f}(b) = 1, \quad (39)$$

and describe how the charge density at a given distance is decomposed over quark flavors. Because the exponential dependence of the individual densities on b cancels between the numerator and denominator, the ratios are of order unity and vary only slowly with b . They can therefore provide direct insight into the changing dynamics at different distances. Figure 11 shows the calculated ratios for the p, Σ^+ and Ξ^0 baryons. The results exhibit several interesting features: (a) At large distances $b > 3$ fm the u and d ratios in all three baryons approach the values $R^{B,u} = 2/3$ and $R^{B,d} = 1/3$, corresponding to u and d quark densities of equal magnitude and opposite sign, Eq. (37), multiplied by the quark charges $2/3$ and $-1/3$. (b) The strange quark fraction drops rapidly with b and is negligible above 2 fm. (c) At distances $b \sim 1$ fm the u and d ratios in the proton attain values that are comparable with the number of u and d valence quarks multiplied by their charge, $R^{p,u} \sim 2 \times 2/3 = 4/3$ and $R^{p,d} \sim 1 \times (-1/3) = -1/3$. Such ratios would be expected in a generic mean-field picture of the motion of valence quarks in the nucleon, in which all quarks occupy the same orbital, and the ratio of the densities is simply determined by their numbers and charges [40]. We emphasize that the present calculation can predict only peripheral densities, and that the

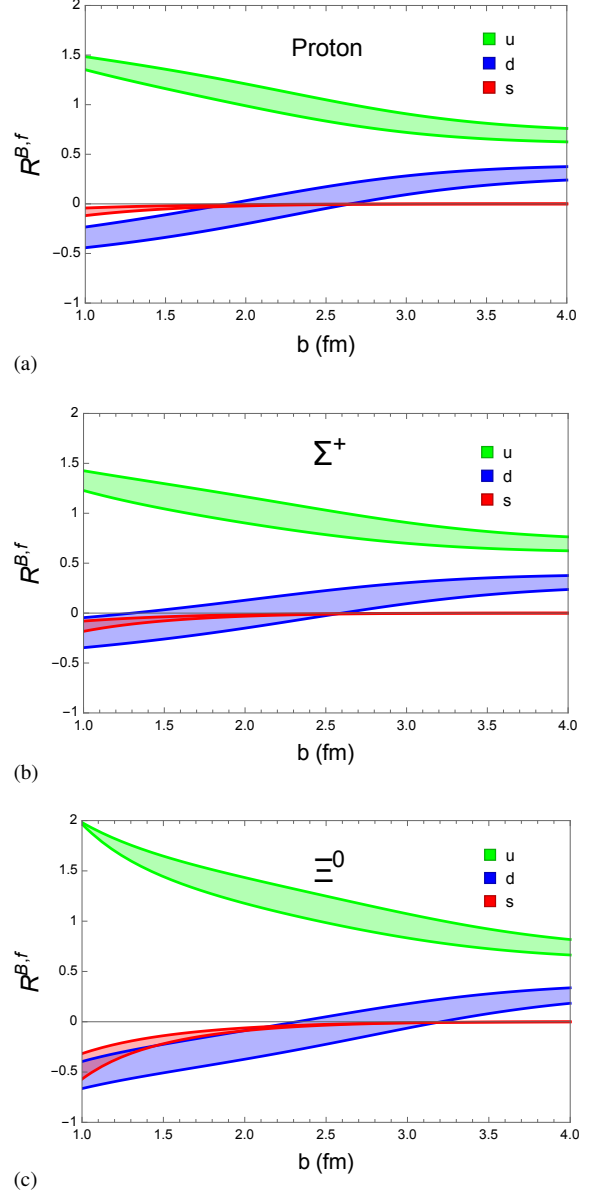


Figure 11: The ratios $R^{B,f}(b)$ ($f = u, d, s$), Eq. (38), describing the relative contribution of each flavor to the total baryon charge density at a given distance b .

accuracy becomes marginal at $b \sim 1$ fm (cf. the discussion in Sec. 2.2). Still it is very reassuring that the ratios thus obtained match with the “quark model” expectations at shorter distances. (d) In the Σ^+ the mean-field picture would predict $R^{\Sigma^+,u} \sim 2 \times 2/3 = 4/3$ and $R^{\Sigma^+,s} \sim 1 \times (-1/3) = -1/3$ for the ratios at small b . Figure 11b shows that the calculated s ratio at $b = 1$ fm is smaller in magnitude than $-1/3$, indicating significant deviations from the mean-field picture at these distances. This conclusion is supported by the presence of a substantial (within errors) non-valence d -quark density at $b = 1$ fm. (e) Similarly, in the Ξ^0 the mean-field picture would imply that $R^{\Xi^0,s}/R^{\Xi^0,u} \sim 2 \times (-1/3)/(2/3) = -1$.⁴ Figure 11c shows that the calculated s/u ratio at $b = 1$ fm is substantially smaller in magnitude than this prediction, and that there is a large non-valence d -quark density. Both observations point to the importance of $\pi^+\Xi^-$ and $\pi^+\Xi^{*-}$ components in the Ξ^0 at distances $b = 1$ fm.

4.3. Isospin breaking effects

Some comments are in order regarding the effect of isospin symmetry breaking on the peripheral baryon densities. In the present study we assume isospin symmetry, which allows us to strictly separate the isovector and isoscalar cuts of the baryon form factors and model the spectral functions accordingly. Baryon structure at distances $b > 2$ fm is dominated by the isovector two-pion cut. If isospin symmetry breaking were included, the isoscalar current would also couple to the two-pion cut (ρ - ω mixing), and the isoscalar density would develop a long-range component. In the baryons where an isovector component is present already in the isospin-symmetric case ($p, n, \Sigma^+, \Sigma^-, \Xi^0, \Xi^-$), the effect of this coupling on the peripheral densities would be negligible. However, in the baryons where the isovector component is absent in the isospin-symmetric case (Σ^0, Λ), the isospin-breaking coupling would qualitatively change the asymptotic behavior of the peripheral densities, resulting in a small long-range component that falls off like the isovector densities produced by the two-pion cut. A rough estimate suggests that this isospin-breaking component should be noticeable only at distances $b > 4$ fm, which are irrelevant for most practical purposes. From a theoretical perspective, though, the long-range structure of the Σ^0 and Λ can provide a sensitive test of isospin breaking effects in baryon structure.

5. Summary and outlook

In this work we have used methods of χ EFT and dispersion analysis to calculate for the first time the peripheral transverse densities of all octet baryons and study their properties. We now want to summarize the main results and insights — methodological and phenomenological — and suggest directions for further study.

⁴The mean-field picture cannot literally be applied to the ratios $R^{B,f}$ if the baryon charge is zero (such as for the Ξ^0), as the total charge density in the denominator of Eq. (38) would be identically zero in this approximation.

On the methodological side, we observed that the transverse densities offer a convenient framework for the dispersive analysis of the baryon form factors, as the contributions from high-mass states at $t \gtrsim 1 \text{ GeV}^2$ are exponentially suppressed and can be controlled by the parameter b . The framework is ideally suited for a dispersive analysis with dynamical input from χ EFT.

The combination of χ EFT with t -channel unitarity significantly improves the χ EFT predictions for the baryon spectral functions on the two-pion cut. The N/D representation of the spectral function in Eq. (25) is natural from the χ EFT perspective, as it separates dynamics governed by the scales M_π and $m_T - m_B$ [in the modified $\pi\pi \rightarrow B\bar{B}$ amplitude $\Gamma_i^B(t)/F_\pi(t)$] from that at the scale Λ_χ [in the pion form factor $[F_\pi(t)]^2$]. The results can be improved systematically by calculating the function $\Gamma_i^B(t)/F_\pi(t)$ to higher orders in the χ EFT expansion.

It would be interesting to study the convergence of the results for the spectral functions when including corrections of $O(\epsilon^4)$ and $O(\epsilon^5)$ in $\Gamma_i^B(t)/F_\pi(t)$. At $O(\epsilon^4)$ the only modifications compared to $O(\epsilon^3)$ are from new $\pi\pi B\bar{B}$ contact terms. At $O(\epsilon^5)$ the $\pi\pi \rightarrow B\bar{B}$ amplitude involves processes with πB intermediate states in addition to the Born diagrams, resulting in a much richer structure. Also, at $O(\epsilon^5)$ $\pi\pi$ rescattering in the t -channel becomes possible, and one should be able to explicitly observe the cancellation of the phase between the numerator and denominator. A calculation of the Λ - Σ transition spectral function in a similar approach was recently reported in Ref. [62].

On the phenomenological side, we found that the octet baryons exhibit a rich peripheral structure as a result of two-pion exchange between the electromagnetic current and the baryon (the ρ meson is included as a $\pi\pi$ resonance within our dispersive approach). Chiral processes with decuplet intermediate states contribute significantly to the isovector spectral functions at $t \sim 30 M_\pi^2 = 0.6 \text{ GeV}^2$ and the densities at $b < 2$ fm. Their contribution qualitatively changes the results compared to octet intermediate states, including the relative strength of the spectral functions or densities in the individual baryons. The inclusion of the decuplet baryons as explicit degrees of freedom in the χ EFT is therefore essential for a realistic description of peripheral baryon structure.

In the nucleon isovector spectral functions and densities, the interplay between N and Δ intermediate states can be explained as a consequence of the large- N_c limit of QCD. N and Δ contributions together are needed for the χ EFT results to satisfy the general N_c -scaling relations, and their relative sign can be inferred in this way [18, 26]. It would be interesting to extend these large- N_c arguments to the spectral functions and densities of the $SU(3)$ octet baryons; see Refs. [77, 78] and references therein. In particular, this might explain why in the strange baryon spectral functions (Σ, Ξ) the contributions from decuplet intermediate states have opposite sign compared to the nucleon spectral functions (N), as seen in Table 1. We plan to address this question in a forthcoming study.

Some comments are in order regarding the comparison of our results with baryon form factor data and empirical densities. For the nucleon (proton and neutron), empirical charge and magnetization densities have been determined by Fourier-

transforming parametrizations of the space-like form factor data; see Ref. [11] for a discussion of the associated uncertainties. In order to reliably extract the peripheral densities at $b > 2$ fm it is essential to use form factor parametrizations with correct analytic properties, as the qualitative behavior in the $b \rightarrow \infty$ limit is governed by the position of the singularities in the complex t -plane. Such parametrizations are provided by dispersive fits to the form factor data as described in Refs. [37, 38, 39], and the resulting peripheral densities are studied in Ref. [40]. In these dispersive fits the isovector spectral functions on the two-pion cut are taken as a theoretical input, and the peripheral densities obtained from the fits just re-express the theoretical input in a different form. The comparison with our results therefore comes down to a theory-vs.-theory comparison of the spectral functions near threshold (or the densities at $b > 2$ fm) as performed in Fig. 7a and c. To improve the situation one should perform dispersive fits to the spacelike form factor data with flexible parametrizations of the isovector spectral functions at $4M_\pi^2 < t < 1 \text{ GeV}^2$ (e.g. with variable strength near the two-pion threshold, and with variable height of the ρ peak), in order to test to what extent the spectral functions in this region could be constrained by spacelike form factor data. Such studies could answer the question how accurately peripheral nucleon structure could be extracted from present and future spacelike form factor data.

The Σ^0 - Λ transition form factor enters in the Dalitz decay $\Sigma^0 \rightarrow \Lambda e^+ e^-$ at timelike momentum transfers $4m_e^2 < t < (m_{\Sigma^0} - m_\Lambda)^2 = 0.006 \text{ GeV}^2$. Precise measurements may be able to determine a combination of the slopes of the magnetic and electric transition form factors at $t = 0$ (magnetic and electric radii). The results could be compared with dispersive calculations of the transition form factors using the spectral functions computed in χ EFT and dispersion theory, cf. Sec. 3.2 and Fig. 8 in this work and Ref. [62]. In the context of transverse densities the slopes of the baryon form factors determine the b^2 -weighted integrals of the densities, $dF_i^B/dt(t=0) = \frac{1}{4} \int d^2b b^2 \rho_i^B(b)$ ($i = 1, 2$), cf. Eq. (2). Because of the weighting with b^2 the integrals receive large contributions from distances $b > 1$ fm and provide sensitive tests of the peripheral densities.

The electromagnetic form factors of the octet baryons are also being studied in lattice QCD [79, 80, 81]. If such calculations could determine the transverse densities at distances $b > 1$ fm, they could be compared directly with the peripheral densities estimated in our χ EFT approach. In fact, comparing (or matching) lattice QCD and χ EFT results at the level of the transverse densities may be very natural, as there should exist a region of “intermediate” distances $b \sim 1$ fm where the densities can be computed reliably in either approach. This possibility deserves further study.

The combination of χ EFT and t -channel unitarity (dispersive improvement) represents a general method that could be applied also to the baryon form factors of other operators with a two-pion cut, such as the scalar current and the energy-momentum tensor. The basic idea and formulas of Sec. 3.2 remain the same, only the $\pi\pi \rightarrow B\bar{B}$ partial-wave amplitude and the pion form factor are replaced by the ones in the partial

waves excited by the other operators [54]. The scalar and tensor operators also have transverse density representations that can be related to the baryons’ partonic structure.

The studies reported here could also be extended to the form factors and transverse densities of the decuplet baryons [82]; in the present calculation they appear only as intermediate states in chiral processes modifying the octet baryon matrix elements. The decuplet baryons are unstable particles with strong decays and finite width. Their electromagnetic form factors can be defined in the context of S -matrix theory, as the residue at the poles in the $\pi N \rightarrow \pi N$ amplitude, and calculated consistently in the framework of relativistic χ EFT [47, 83]. The transverse densities associated with the Δ form factors are of special interest because new angular structures appear in the spin-3/2 states [cf. Eq. (5) for the spin-1/2 states]. They are also of relevance for exploring the large- N_c limit of QCD, where the N and Δ become degenerate and can be viewed as rotational states of a classical mean-field solution [84]. The N - Δ transition form factors are measured in resonance electroproduction experiments and can be described in terms of transition densities [9, 85]. The form factors of decuplet baryons are studied also in lattice QCD [86, 87, 88].

We expect that the methods used here will lead to more predictive studies of baryon form factors in χ EFT, and at the same time extend its range of applicability to higher energies.

Appendix A. Validation of EFT calculations

To validate the χ EFT calculations we have computed the octet baryon form factors themselves from the full set of $\mathcal{O}(\epsilon^3)$ diagrams, even though only the t -channel cut diagrams of Fig. 4a, b and c are needed for our study of peripheral densities. Our results for the nucleon form factors fully reproduce those of Ref. [47] when reduced to the $SU(2)$ flavor case, which is done by setting the contribution of the kaon loops to zero. The $SU(2)$ coupling constants g_A and h_A correspond to the $SU(3)$ constants $D + F$ and $-2\sqrt{2}C$, respectively. We have also verified current conservation (electromagnetic gauge invariance) with the $\mathcal{O}(\epsilon^3)$ results for the current matrix element.

The χ EFT calculations were independently performed with two different methods: the analytic calculations were first done with the help of FORM [89, 90], and then separately with FeynCalc [91, 92]. The two methods give the same numerical results.

Appendix B. Off-shell properties of spin-3/2 EFT

The χ EFT used in the present study includes spin-3/2 decuplet baryons as dynamical degrees of freedom. In this appendix we comment on issues related to the off-shell properties of the EFT with spin-3/2 fields and compare our results to earlier calculations of transverse densities including the Δ isobar [18, 26].

The formulation of a relativistic quantum field theory with spin-3/2 fermions is inherently not unique. Relativistic invariance necessitates working with “redundant” fields containing spin-1/2 and spin-3/2 degrees of freedom, and the projection on

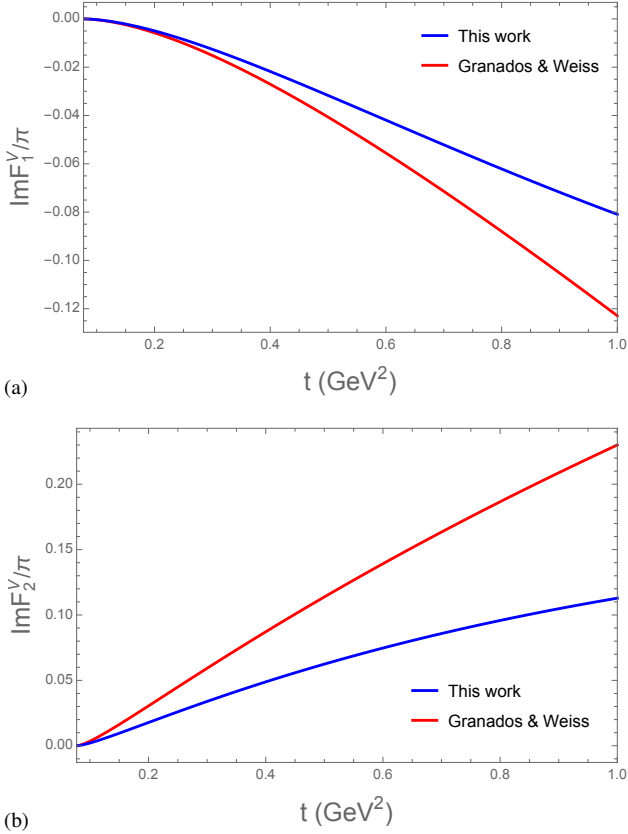


Figure B.12: Comparison of the Δ contribution to the nucleon isovector spectral functions $\text{Im}F_i^V(t)$ ($i = 1, 2$) obtained in Refs. [18, 26] and the present work. The curves show the total contribution resulting from the Δ triangle graph, Fig. 4c, which includes the “intermediate Δ ” and “contact” terms described in Refs. [18, 26] and in the text.

physical spin-3/2 degrees of freedom can be performed unambiguously only on the mass shell, resulting in an ambiguity in the definition of the propagator and the vertices off the mass-shell [65, 66]. The ambiguity can be formalized as an invariance under point transformations [69, 93]. In the context of EFT it is contained in the overall reparametrization invariance — the freedom to redefine the field variables, changing the off-shell behavior of the propagators and vertices, but leaving the on-shell amplitudes invariant. On-shell amplitudes calculated in EFTs with different choices of fields agree in the parametric order to which they were calculated but can differ by higher-order terms. The latter can give rise to numerical differences if the EFT expressions are used for numerical approximation.

In Refs. [18, 26] the spectral functions of the nucleon form factors were computed in a relativistic χ EFT with spin-3/2 Δ fields, using a Rarita-Schwinger propagator for the Δ , and the minimal form of the $\pi N\Delta$ vertex without explicit off-shell terms. The Feynman integrals obtained from the triangle diagrams with intermediate Δ were separated into two parts:

- (i) An “intermediate Δ ” term, which results from the singularity of the integrand at the Δ pole and can be evaluated by contour integration with the residue at the Δ pole. This part of the spectral functions corresponds to the triple-cut

Feynman diagram in which both the exchanged pions and the intermediate Δ are on mass-shell. It contains the sub-threshold singularity at $t < 4M_\pi^2 - (m_\Delta^2 - m_N^2 + M_\pi^2)^2/M_\pi^2$ (or the left-hand cut of the $\pi\pi \rightarrow N\bar{N}$ amplitude), as represented by the arctangent function in Eqs. (4.21) and (4.23) of Ref. [18], as well as certain polynomial terms in t .

- (ii) A “contact” term, which results from the parts of the integrand that are non-singular at the Δ pole. This term leads to an integral of the same form as that resulting from the diagram with a $\pi\pi NN$ contact term in the Lagrangian, and can be combined with the latter.

The separation is performed unambiguously within the reduction procedure described in Refs. [18, 26]. It is physically natural because (a) the intermediate Δ term does not depend on the off-shell behavior of the χ EFT, and the off-shell ambiguity is localized entirely in the contact term; (b) the intermediate Δ term can be represented in light-front time-ordered form, as an overlap integral of light-front wave functions describing the transition of the external N to a $\pi\Delta$ intermediate state and back [26]; (c) the scaling behavior of the intermediate Δ and contact terms in the large- N_c limit matches that of the corresponding terms in contributions with intermediate N states.

In the present work we use a relativistic χ EFT with spin-3/2 Δ fields with consistent $\pi N\Delta$ vertices, which are constructed to be invariant under point transformations by making use of the Heisenberg equations of motion of the fields. This choice of vertices corresponds to a different off-shell behavior from that used in Refs. [18, 26]. It is instructive to compare the results for the spectral functions obtained with the two schemes. We find that: (a) The intermediate Δ terms of the spectral functions (as defined above and in Refs. [18, 26]) are identical in the two schemes. This confirms explicitly that these terms are independent of the off-shell behavior of the χ EFT. (b) The contact terms obtained in the two schemes are identical at $\mathcal{O}(\epsilon^3)$, which is the accuracy of the present calculation, but differ in higher-order contributions. In $\text{Im}F_1$ the differences appear at $\mathcal{O}(\epsilon^5)$ (two orders higher than the nominal order), while in $\text{Im}F_2$ they appear at $\mathcal{O}(\epsilon^4)$ (one order higher than the nominal order). This shows that the off-shell ambiguity manifests itself in the contact terms at the expected order.

In Fig. B.12 we compare the numerical results for the total Δ contribution to the nucleon spectral functions (including both the intermediate Δ and contact terms) obtained in Ref. [18] and the present calculation. One sees that the results have similar behavior in the near-threshold region but show significant differences at higher masses: $\sim 20\%$ difference in $\text{Im}F_1$ at $t = 0.6 \text{ GeV}^2$, and $\sim 50\%$ in $\text{Im}F_2$. The pattern is consistent with the parametric orders of the differences (see above). As noted above, these differences are entirely due to the different contact terms in the spectral functions and could be compensated by adding explicit $\pi\pi NN$ contact terms to the Lagrangian. Since the setup of Ref. [18] uses an arbitrary off-shell behavior, while the present formulation uses consistent vertices and can be extended to higher-order calculations, we consider the results of the present calculation more significant and use them in our study.

Altogether, the comparison with Ref. [18] shows that the $O(\epsilon^3)$ results for the spectral functions are independent of the off-shell behavior of the χ EFT, as it should be. Differences between schemes appear only in higher-order contributions and could be compensated by adding explicit $\pi\pi NN$ contact terms to the Lagrangian.

Appendix C. Isoscalar vector meson couplings

In this appendix we estimate the couplings of the isoscalar vector mesons (ω, ϕ) to the $SU(3)$ octet baryons and describe the parameters in our model for the isoscalar spectral function, Eq. (30). Our treatment follows the approach of Ref. [94] and makes use of $SU(3)$ symmetry, certain assumptions about the F/D ratios, and empirical meson-nucleon couplings. The coupling of the vector mesons to the octet baryons is described by the phenomenological Lagrangian density [95]

$$\begin{aligned} \mathcal{L}_{VBB} = & -g_{VBB}\bar{B}\gamma^\mu BV_\mu \\ & -\frac{if_{VBB}}{4m_N}\bar{B}\sigma^{\mu\nu}B(\partial_\mu V_\nu - \partial_\nu V_\mu), \end{aligned} \quad (\text{C.1})$$

where B is the baryon field, V_μ is the vector meson field, and g_{VBB} and f_{VBB} are the vector and tensor couplings. In the case of $SU(3)$ symmetry the flavor structure of the couplings is of the general form

$$\begin{aligned} g_{VBB} \rightarrow & g_F \text{Tr}(\bar{B}\{V_8, B\}) + g_D \text{Tr}(\bar{B}[V_8, B]) \\ & + g_S V_1 \text{Tr}(\bar{B}B), \end{aligned} \quad (\text{C.2})$$

where g_F and g_D are the symmetric and antisymmetric $\mathbf{8}\times\mathbf{8} \rightarrow \mathbf{8}$ couplings, and g_S is the $\mathbf{8}\times\mathbf{8} \rightarrow \mathbf{1}$ coupling; a similar relation expresses f_{VBB} in terms of f_F, f_D and f_S . Here B is the octet baryon field Eq. (15), V_8 is the octet vector meson field [cf. Eq. (14)],

$$V_8 = \begin{pmatrix} \frac{1}{\sqrt{2}}\rho^0 + \frac{1}{\sqrt{6}}\omega_8 & \rho^+ & K^{*+} \\ \rho^- & -\frac{1}{\sqrt{2}}\rho^0 + \frac{1}{\sqrt{6}}\omega_8 & K^{*0} \\ K^{*-} & \bar{K}^{*0} & -\frac{2}{\sqrt{6}}\omega_8 \end{pmatrix}, \quad (\text{C.3})$$

and $V_1 = \omega_1$ is the singlet vector meson field. Eq. (C.2) encodes the constraints of $SU(3)$ symmetry on the physical VBB couplings. Here we are interested in the couplings of the neutral isoscalar vector mesons, ω and ϕ . Assuming ideal mixing, the physical ω and ϕ fields are related to the octet and singlet fields by⁵

$$\omega = \frac{1}{\sqrt{3}}\omega_8 + \sqrt{\frac{2}{3}}\omega_1, \quad (\text{C.4})$$

$$\phi = \sqrt{\frac{2}{3}}\omega_8 - \frac{1}{\sqrt{3}}\omega_1. \quad (\text{C.5})$$

⁵In our convention the quark representation of the meson states is $|\omega\rangle = (|\bar{u}u\rangle + |\bar{d}d\rangle)/\sqrt{2}$ and $|\phi\rangle = -|\bar{s}s\rangle$. The ϕ coupling to the electromagnetic current is positive, while the ϕpp vector coupling for standard parameters is negative (see below).

The couplings of the physical mesons to the baryons can then be determined by expressing the Lagrangian Eq. (C.1) in terms of the physical fields.

To determine the values of the $SU(3)$ couplings we use empirical information on the couplings of the non-strange vector mesons to the nucleon (ρ^0, ω), and theoretical assumptions about the F/D ratios. The $\rho^0 NN$ and ωNN couplings are related to the $SU(3)$ couplings as

$$g_{\rho^0 pp} = \frac{1}{\sqrt{2}}(g_F + g_D), \quad (\text{C.6})$$

$$g_{\omega pp} = \frac{3g_F - g_D}{3\sqrt{2}} + \sqrt{\frac{2}{3}}g_S, \quad (\text{C.7})$$

$$f_{\rho^0 pp} = \frac{1}{\sqrt{2}}(f_F + f_D) \quad (\text{C.8})$$

$$f_{\omega pp} = \frac{3f_F - f_D}{3\sqrt{2}} + \sqrt{\frac{2}{3}}f_S \quad (\text{C.9})$$

Assuming that the baryons' electromagnetic couplings are dominated by their coupling to vector mesons (vector meson dominance), the ratios of the baryon electric charges and magnetic moments (or their $SU(6)$ relations) provide two conditions on the ratio of F and D couplings [94],

$$\frac{g_F}{g_F + g_D} = 1, \quad (\text{C.10})$$

$$\frac{g_F + f_F}{g_F + f_F + g_D + f_D} = \frac{2}{5}. \quad (\text{C.11})$$

Equations (C.6)–(C.11) allow us to calculate the values of the $SU(3)$ couplings in terms of the empirical $\rho^0 pp$ and ωpp vector and tensor couplings. Using the couplings determined by the meson exchange model of the nucleon-nucleon interaction [95],

$$\left. \begin{aligned} g_{\rho^0 pp} &= 3.25, & f_{\rho^0 pp} &= 19.8, \\ g_{\omega pp} &= 15.9, & f_{\omega pp} &= 0, \end{aligned} \right\} \quad (\text{C.12})$$

we obtain

$$\left. \begin{aligned} g_F &= 4.6, & f_F &= 8.4, \\ g_D &= 0, & f_D &= 19.6, \\ g_S &= 15.5, & f_S &= -1.6. \end{aligned} \right\} \quad (\text{C.13})$$

The coupling of the vector mesons to the electromagnetic current is summarized by the current-field identity

$$J_\mu = \sum_{V=\rho,\omega,\phi} \frac{M_V^2}{F_V} V_\mu. \quad (\text{C.14})$$

The constants F_V parametrize the coupling strength and can be inferred from the e^+e^- decay widths of the vector mesons, $\Gamma(V \rightarrow e^+e^-) = (\alpha M_V/3)(e/F_V)^2$, where $\alpha = e^2/(4\pi) \approx 1/137$ is the fine structure constant. For the ω we obtain $F_\omega = 16.7$ and

$$M_\omega^2/F_\omega = 0.037, \quad (\text{C.15})$$

using $M_\omega = 783$ MeV and the width from Ref. [96]. The ϕ meson coupling is then fixed by assuming that the ratio of ω and ϕ electromagnetic couplings follow their valence quark content

[this assumption was used already in the vector dominance relations Eqs. (C.10) and (C.11)],

$$(M_\phi^2/F_\phi) : (M_\omega^2/F_\omega) = \sqrt{2} : 1, \quad (\text{C.16})$$

which gives $M_\phi^2/F_\phi = 0.052$. Note that F_V is positive in our convention. The parameters in the vector meson pole parametrization of the isoscalar spectral function Eq. (30) ($V = \omega, \phi$) are then calculated from the vector meson-baryon couplings and the electromagnetic couplings as

$$a_1^{VBB} = \frac{g_{VBB}M_V^2}{F_V}, \quad a_2^{VBB} = \frac{f_{VBB}M_V^2}{F_V}. \quad (\text{C.17})$$

The results obtained for the various octet baryon states are shown in Table C.2.

With the $g_{\rho^0 pp}$ and $g_{\omega pp}$ couplings of Ref. [95] (see above) the present model gives a small negative value of $g_{\phi NN}$, as was obtained in earlier studies; see Ref. [94] and references therein. We note that the present model could also accommodate the ‘‘quark model’’ value $g_{\phi NN} = 0$, which would be obtained with $g_{\omega pp} = 3g_{\rho^0 pp}$; see Ref. [94] for discussion. We emphasize that the ϕ meson couplings to the strange octet baryons are generated by $SU(3)$ symmetry regardless of the precise value of $g_{\phi NN}$, and that we are not aiming for an accurate description of the strange form factors of the nucleon in the present study.

To estimate the uncertainty of our parametrization of the isoscalar form factors we replace the fixed $g_{\omega pp}$ and $f_{\omega pp}$ values of Ref. [95] by the range of values extracted from a fit to the isoscalar nucleon form factor data [38],

$$g_{\omega pp} = 16.7 \dots 23.1, \quad f_{\omega pp} = -3.6 \dots + 10.3, \quad (\text{C.18})$$

and follow the variation of the results over the allowed range. The couplings obtained in this way are shown in Table C.3.

Acknowledgments

We thank Ina Lorenz for providing us with the parametrization of the pion form factor, and Ulf-G. Meißner for discussions and support during the early stages of this project. This material is based upon work supported by the U.S. Department of Energy, Office of Science, Office of Nuclear Physics under contract DE-AC05-06OR23177. We acknowledge partial financial support from the Deutsche Forschungsgemeinschaft (Sino-German CRC 110), MINECO (Spain) and the ERDF (European Commission) grants No. FPA2013-40483-P, FIS2014-51948-C2-2-P and SEV-2014-0398. This work was also supported by the Generalitat Valenciana under Contract PROMETEOII/2014/0068.

References

- [1] P. A. M. Dirac, *Rev. Mod. Phys.* **21**, 392 (1949). doi:10.1103/RevModPhys.21.392
- [2] H. Leutwyler and J. Stern, *Annals Phys.* **112**, 94 (1978). doi:10.1016/0003-4916(78)90082-9
- [3] G. P. Lepage and S. J. Brodsky, *Phys. Rev. D* **22**, 2157 (1980). doi:10.1103/PhysRevD.22.2157

- [4] S. J. Brodsky, H. C. Pauli and S. S. Pinsky, *Phys. Rept.* **301**, 299 (1998) doi:10.1016/S0370-1573(97)00089-6 [hep-ph/9705477].
- [5] D. E. Soper, *Phys. Rev. D* **15**, 1141 (1977). doi:10.1103/PhysRevD.15.1141
- [6] M. Burkardt, *Phys. Rev. D* **62**, 071503 (2000) Erratum: [*Phys. Rev. D* **66**, 119903 (2002)] doi:10.1103/PhysRevD.62.071503, 10.1103/PhysRevD.66.119903 [hep-ph/0005108].
- [7] M. Burkardt, *Int. J. Mod. Phys. A* **18**, 173 (2003) doi:10.1142/S0217751X03012370 [hep-ph/0207047].
- [8] G. A. Miller, *Phys. Rev. Lett.* **99**, 112001 (2007) doi:10.1103/PhysRevLett.99.112001 [arXiv:0705.2409 [nucl-th]].
- [9] C. E. Carlson and M. Vanderhaeghen, *Phys. Rev. Lett.* **100**, 032004 (2008) doi:10.1103/PhysRevLett.100.032004 [arXiv:0710.0835 [hep-ph]].
- [10] M. Vanderhaeghen and T. Walcher, *Nucl. Phys. News* **21**, 14 (2011) doi:10.1080/10619127.2011.554757 [arXiv:1008.4225 [hep-ph]].
- [11] S. Venkat, J. Arrington, G. A. Miller and X. Zhan, *Phys. Rev. C* **83**, 015203 (2011) doi:10.1103/PhysRevC.83.015203 [arXiv:1010.3629 [nucl-th]].
- [12] G. A. Miller, *Phys. Rev. C* **80**, 045210 (2009) doi:10.1103/PhysRevC.80.045210 [arXiv:0908.1535 [nucl-th]].
- [13] G. A. Miller, *Ann. Rev. Nucl. Part. Sci.* **60**, 1 (2010) doi:10.1146/annurev.nucl.012809.104508 [arXiv:1002.0355 [nucl-th]].
- [14] M. Diehl, *Eur. Phys. J. C* **25**, 223 (2002) Erratum: [*Eur. Phys. J. C* **31**, 277 (2003)] doi:10.1007/s10052-002-1016-9 [hep-ph/0205208].
- [15] A. V. Belitsky and A. V. Radyushkin, *Phys. Rept.* **418**, 1 (2005) doi:10.1016/j.physrep.2005.06.002 [hep-ph/0504030].
- [16] S. Boffi and B. Pasquini, *Riv. Nuovo Cim.* **30**, 387 (2007) doi:10.1393/ncr/i2007-10025-7 [arXiv:0711.2625 [hep-ph]].
- [17] M. Strikman and C. Weiss, *Phys. Rev. C* **82**, 042201 (2010) doi:10.1103/PhysRevC.82.042201 [arXiv:1004.3535 [hep-ph]].
- [18] C. Granados and C. Weiss, *JHEP* **1401**, 092 (2014) doi:10.1007/JHEP01(2014)092 [arXiv:1308.1634 [hep-ph]].
- [19] J. Gasser and H. Leutwyler, *Annals Phys.* **158**, 142 (1984). doi:10.1016/0003-4916(84)90242-2
- [20] J. Gasser and H. Leutwyler, *Nucl. Phys. B* **250**, 465 (1985). doi:10.1016/0550-3213(85)90492-4
- [21] V. Bernard, N. Kaiser and U. G. Meissner, *Int. J. Mod. Phys. E* **4**, 193 (1995) doi:10.1142/S0218301395000092 [hep-ph/9501384].
- [22] S. Scherer, *Adv. Nucl. Phys.* **27**, 277 (2003) [hep-ph/0210398].
- [23] S. Scherer and M. R. Schindler, *Lect. Notes Phys.* **830**, 1 (2012) doi:10.1007/978-3-642-19254-8-1
- [24] C. Granados and C. Weiss, *JHEP* **1507**, 170 (2015) doi:10.1007/JHEP07(2015)170 [arXiv:1503.04839 [hep-ph]].
- [25] C. Granados and C. Weiss, *Phys. Rev. C* **92**, no. 2, 025206 (2015) doi:10.1103/PhysRevC.92.025206 [arXiv:1503.02055 [hep-ph]].
- [26] C. Granados and C. Weiss, *JHEP* **1606**, 075 (2016) doi:10.1007/JHEP06(2016)075 [arXiv:1603.08881 [hep-ph]].
- [27] J. Gasser, M. E. Sainio and A. Svarc, *Nucl. Phys. B* **307**, 779 (1988). doi:10.1016/0550-3213(88)90108-3
- [28] V. Bernard, N. Kaiser and U. G. Meissner, *Nucl. Phys. A* **611**, 429 (1996) doi:10.1016/S0375-9474(96)00291-6 [hep-ph/9607428].
- [29] T. Becher and H. Leutwyler, *Eur. Phys. J. C* **9**, 643 (1999) doi:10.1007/PL00021673 [hep-ph/9901384].
- [30] B. Kubis and U. G. Meissner, *Nucl. Phys. A* **679**, 698 (2001) doi:10.1016/S0375-9474(00)00378-X [hep-ph/0007056].
- [31] N. Kaiser, *Phys. Rev. C* **68**, 025202 (2003) doi:10.1103/PhysRevC.68.025202 [nucl-th/0302072].
- [32] W. R. Frazer and J. R. Fulco, *Phys. Rev.* **117**, 1603 (1960). doi:10.1103/PhysRev.117.1603
- [33] W. R. Frazer and J. R. Fulco, *Phys. Rev.* **117**, 1609 (1960). doi:10.1103/PhysRev.117.1609
- [34] G. Hohler and E. Pietarinen, *Nucl. Phys. B* **95**, 210 (1975). doi:10.1016/0550-3213(75)90042-5
- [35] M. A. Belushkin, H.-W. Hammer and U. G. Meissner, *Phys. Lett. B* **633**, 507 (2006) doi:10.1016/j.physletb.2005.12.053 [hep-ph/0510382].
- [36] M. Hoferichter, B. Kubis, J. Ruiz de Elvira, H.-W. Hammer and U.-G. Meissner, *Eur. Phys. J. A* **52**, no. 11, 331 (2016) doi:10.1140/epja/i2016-16331-7 [arXiv:1609.06722 [hep-ph]].
- [37] G. Hohler, E. Pietarinen, I. Sabba Stefanescu, F. Borkowski, G. G. Simon, V. H. Walther and R. D. Wendling, *Nucl. Phys. B* **114** (1976) 505.

Couplings [GeV ²]				
B	$a_1^{\omega BB}$	$a_1^{\phi BB}$	$a_2^{\omega BB}$	$a_2^{\phi BB}$
p, n	0.58	-0.23	0	0.14
Λ	0.46	-0.46	-0.39	-0.63
Σ^\pm, Σ^0	0.46	-0.46	0.29	0.73
$\Lambda - \Sigma^0$	0	0	0	0
Ξ^0, Ξ^-	0.35	-0.70	-0.44	-0.73

Table C.2: Parameters of the vector meson pole parametrization of the isoscalar octet baryon form factors, Eq. (C.17), obtained from $SU(3)$ symmetry and F/D ratio models, Eqs. (C.6)–(C.11), and empirical ρpp and ωpp couplings. This set uses the ρpp and ωpp couplings from the meson exchange parametrization of the NN interaction of Ref. [95], Eq. (C.12). The couplings of the vector mesons to the electromagnetic current are from Eqs. (C.15) and (C.16).

Couplings [GeV ²]				
B	$a_1^{\omega BB}$	$a_1^{\phi BB}$	$a_2^{\omega BB}$	$a_2^{\phi BB}$
p, n	(0.61, 0.85)	(-0.49, 0.26)	(-0.13, 0.38)	(-0.23, 0.28)
Λ	(0.49, 0.73)	(-0.73, 0.49)	(-0.52, -0.01)	(-1.01, -0.49)
Σ^\pm, Σ^0	(0.49, 0.73)	(-0.73, 0.49)	(0.16, 0.67)	(0.35, 0.86)
$\Lambda - \Sigma^0$	0	0	0	0
Ξ^0, Ξ^-	(0.37, 0.61)	(-0.97, -0.73)	(-0.57, -0.06)	(-1.11, -0.59)

Table C.3: Parameters of the vector meson pole parametrization of the isoscalar octet baryon form factors, Eq. (C.17), obtained from $SU(3)$ symmetry and models of the F/D ratios, Eqs. (C.6)–(C.11), and empirical ρpp and ωpp couplings (cf. Table C.2). This set uses the range of ωpp couplings extracted from the fit to the nucleon form factor data of Ref. [38], Eq. (C.18).

- doi:10.1016/0550-3213(76)90449-1
- [38] M. A. Belushkin, H.-W. Hammer and U.-G. Meissner, Phys. Rev. C **75**, 035202 (2007) doi:10.1103/PhysRevC.75.035202 [hep-ph/0608337].
- [39] I. T. Lorenz, H.-W. Hammer and U. G. Meissner, Eur. Phys. J. A **48**, 151 (2012) doi:10.1140/epja/i2012-12151-1 [arXiv:1205.6628 [hep-ph]].
- [40] G. A. Miller, M. Strikman and C. Weiss, Phys. Rev. C **84**, 045205 (2011) doi:10.1103/PhysRevC.84.045205 [arXiv:1105.6364 [hep-ph]].
- [41] T. Fuchs, J. Gegelia, G. Japaridze and S. Scherer, Phys. Rev. D **68**, 056005 (2003) doi:10.1103/PhysRevD.68.056005 [hep-ph/0302117].
- [42] T. Becher and H. Leutwyler, JHEP **0106**, 017 (2001) doi:10.1088/1126-6708/2001/06/017 [hep-ph/0103263].
- [43] J. M. Alarcon, J. Martin Camalich, J. A. Oller and L. Alvarez-Ruso, Phys. Rev. C **83**, 055205 (2011) Erratum: [Phys. Rev. C **87**, no. 5, 059901 (2013)] doi:10.1103/PhysRevC.83.055205, 10.1103/PhysRevC.87.059901 [arXiv:1102.1537 [nucl-th]].
- [44] J. M. Alarcon, J. Martin Camalich and J. A. Oller, Annals Phys. **336**, 413 (2013). doi:10.1016/j.aop.2013.06.001 [arXiv:1210.4450 [hep-ph]].
- [45] V. Lensky, J. M. Alarcon and V. Pascalutsa, Phys. Rev. C **90**, no. 5, 055202 (2014) doi:10.1103/PhysRevC.90.055202 [arXiv:1407.2574 [hep-ph]].
- [46] A. N. Hiller Blin, T. Ledwig and M. J. Vicente Vacas, Phys. Rev. D **93**, no. 9, 094018 (2016) doi:10.1103/PhysRevD.93.094018 [arXiv:1602.08967 [hep-ph]].
- [47] T. Ledwig, J. Martin-Camalich, V. Pascalutsa and M. Vanderhaeghen, Phys. Rev. D **85**, 034013 (2012) doi:10.1103/PhysRevD.85.034013 [arXiv:1108.2523 [hep-ph]].
- [48] L. S. Geng, J. Martin Camalich, L. Alvarez-Ruso and M. J. Vicente Vacas, Phys. Rev. Lett. **101**, 222002 (2008) doi:10.1103/PhysRevLett.101.222002 [arXiv:0805.1419 [hep-ph]].
- [49] T. Ledwig, J. Martin Camalich, L. S. Geng and M. J. Vicente Vacas, Phys. Rev. D **90**, no. 5, 054502 (2014) doi:10.1103/PhysRevD.90.054502 [arXiv:1405.5456 [hep-ph]].
- [50] J. M. Alarcon, J. Martin Camalich and J. A. Oller, Phys. Rev. D **85**, 051503 (2012) doi:10.1103/PhysRevD.85.051503 [arXiv:1110.3797 [hep-ph]].
- [51] J. M. Alarcon, L. S. Geng, J. Martin Camalich and J. A. Oller, Phys. Lett. B **730**, 342 (2014) doi:10.1016/j.physletb.2014.01.065 [arXiv:1209.2870 [hep-ph]].
- [52] J. M. Alarcon, V. Lensky and V. Pascalutsa, Eur. Phys. J. C **74**, no. 4, 2852 (2014) doi:10.1140/epjc/s10052-014-2852-0 [arXiv:1312.1219 [hep-ph]].
- [53] K. M. Watson, Phys. Rev. **95**, 228 (1954). doi:10.1103/PhysRev.95.228
- [54] J. M. Alarcon and C. Weiss, in preparation.
- [55] G. F. Chew and S. Mandelstam, Phys. Rev. **119**, 467 (1960). doi:10.1103/PhysRev.119.467
- [56] J. A. Oller and E. Oset, Phys. Rev. D **60**, 074023 (1999) doi:10.1103/PhysRevD.60.074023 [hep-ph/9809337].
- [57] J. A. Oller, E. Oset and A. Ramos, Prog. Part. Nucl. Phys. **45**, 157 (2000) doi:10.1016/S0146-6410(00)00104-6 [hep-ph/0002193].
- [58] U. G. Meissner and J. A. Oller, Nucl. Phys. A **673**, 311 (2000) doi:10.1016/S0375-9474(00)00150-0 [nucl-th/9912026].
- [59] J. A. Oller and U. G. Meissner, Phys. Lett. B **500**, 263 (2001) doi:10.1016/S0370-2693(01)00078-8 [hep-ph/0011146].
- [60] M. Albaladejo and J. A. Oller, Phys. Rev. C **84**, 054009 (2011) doi:10.1103/PhysRevC.84.054009 [arXiv:1107.3035 [nucl-th]].
- [61] M. Albaladejo and J. A. Oller, Phys. Rev. C **86**, 034005 (2012) doi:10.1103/PhysRevC.86.034005 [arXiv:1201.0443 [nucl-th]].
- [62] C. Granados, S. Leupold and E. Perotti, arXiv:1701.09130 [hep-ph].
- [63] J. M. Alarcon, A. N. H. Blin and C. Weiss, Few Body Syst. **58**, no. 3, 121 (2017) doi:10.1007/s00601-017-1283-5 [arXiv:1701.05871 [hep-ph]].
- [64] V. Pascalutsa, Phys. Rev. D **58**, 096002 (1998) doi:10.1103/PhysRevD.58.096002 [hep-ph/9802288];
- [65] V. Pascalutsa and R. Timmermans, Phys. Rev. C **60**, 042201 (1999) doi:10.1103/PhysRevC.60.042201 [nucl-th/9905065];
- [66] V. Pascalutsa, Phys. Lett. B **503**, 85 (2001) doi:10.1016/S0370-2693(01)00140-X [hep-ph/0008026].
- [67] H. Krebs, E. Epelbaum and U. G. Meissner, Phys. Rev. C **80**, 028201 (2009) doi:10.1103/PhysRevC.80.028201 [arXiv:0812.0132 [hep-th]].
- [68] T. R. Hemmert, B. R. Holstein and J. Kambor, Phys. Lett. B **395**, 89 (1997) doi:10.1016/S0370-2693(97)00049-X [hep-ph/9606456].
- [69] T. R. Hemmert, B. R. Holstein and J. Kambor, J. Phys. G **24**, 1831 (1998) doi:10.1088/0954-3899/24/10/003 [hep-ph/9712496].
- [70] G. J. Gounaris and J. J. Sakurai, Phys. Rev. Lett. **21** (1968) 244. doi:10.1103/PhysRevLett.21.244
- [71] L. M. Barkov *et al.*, Nucl. Phys. B **256**, 365 (1985). doi:10.1016/0550-3213(85)90399-2
- [72] R. Karplus, C. M. Sommerfield and E. H. Wichmann, Phys. Rev. **111**, 1187 (1958). doi:10.1103/PhysRev.111.1187
- [73] L. D. Landau, Nucl. Phys. **13**, 181 (1959). doi:10.1016/0029-5582(59)90154-3

- [74] H. W. Hammer and M. J. Ramsey-Musolf, Phys. Rev. C **60**, 045205 (1999) Erratum: [Phys. Rev. C **62**, 049903 (2000)] doi:10.1103/PhysRevC.60.045205, 10.1103/PhysRevC.62.049903 [hep-ph/9812261].
- [75] H. W. Hammer and M. J. Ramsey-Musolf, Phys. Rev. C **60**, 045204 (1999) Erratum: [Phys. Rev. C **62**, 049902 (2000)] doi:10.1103/PhysRevC.60.045204, 10.1103/PhysRevC.62.049902 [hep-ph/9903367].
- [76] U. G. Meissner, V. Mull, J. Speth and J. W. van Orden, Phys. Lett. B **408**, 381 (1997) doi:10.1016/S0370-2693(97)00828-9 [hep-ph/9701296].
- [77] R. Flores-Mendieta and J. L. Goity, Phys. Rev. D **90**, no. 11, 114008 (2014) doi:10.1103/PhysRevD.90.114008 [arXiv:1407.0926 [hep-ph]].
- [78] R. Flores-Mendieta and M. A. Rivera-Ruiz, Phys. Rev. D **92**, no. 9, 094026 (2015) doi:10.1103/PhysRevD.92.094026 [arXiv:1511.02932 [hep-ph]].
- [79] H. W. Lin and K. Orginos, Phys. Rev. D **79**, 074507 (2009) doi:10.1103/PhysRevD.79.074507 [arXiv:0812.4456 [hep-lat]].
- [80] P. E. Shanahan *et al.* [CSSM and QCDSF/UKQCD Collaborations], Phys. Rev. D **89**, 074511 (2014) doi:10.1103/PhysRevD.89.074511 [arXiv:1401.5862 [hep-lat]].
- [81] P. E. Shanahan *et al.*, Phys. Rev. D **90**, 034502 (2014) doi:10.1103/PhysRevD.90.034502 [arXiv:1403.1965 [hep-lat]].
- [82] J. M. Alarcón *et al.*, in preparation.
- [83] T. Ledwig, V. Pascalutsa and M. Vanderhaeghen, Phys. Rev. D **82**, 091301 (2010) doi:10.1103/PhysRevD.82.091301 [arXiv:1004.5055 [hep-ph]].
- [84] G. S. Adkins, C. R. Nappi and E. Witten, Nucl. Phys. B **228**, 552 (1983).
- [85] V. Pascalutsa and M. Vanderhaeghen, Phys. Rev. D **76**, 111501 (2007) doi:10.1103/PhysRevD.76.111501 [arXiv:0711.0147 [hep-ph]].
- [86] C. Alexandrou *et al.*, Phys. Rev. D **79**, 014507 (2009) doi:10.1103/PhysRevD.79.014507 [arXiv:0810.3976 [hep-lat]].
- [87] C. Aubin, K. Orginos, V. Pascalutsa and M. Vanderhaeghen, Phys. Rev. D **79**, 051502 (2009) doi:10.1103/PhysRevD.79.051502 [arXiv:0811.2440 [hep-lat]].
- [88] C. Alexandrou, T. Korzec, G. Koutsou, C. Lorce, J. W. Negele, V. Pascalutsa, A. Tsapalis and M. Vanderhaeghen, Nucl. Phys. A **825**, 115 (2009) doi:10.1016/j.nuclphysa.2009.04.005 [arXiv:0901.3457 [hep-ph]].
- [89] J. A. M. Vermaseren, math-ph/0010025.
- [90] J. Kuipers, T. Ueda, J. A. M. Vermaseren and J. Volla, Comput. Phys. Commun. **184**, 1453 (2013) doi:10.1016/j.cpc.2012.12.028 [arXiv:1203.6543 [cs.SC]].
- [91] R. Mertig, M. Bohm and A. Denner, Comput. Phys. Commun. **64**, 345 (1991). doi:10.1016/0010-4655(91)90130-D
- [92] V. Shtabovenko, R. Mertig and F. Orellana, Comput. Phys. Commun. **207**, 432 (2016) doi:10.1016/j.cpc.2016.06.008 [arXiv:1601.01167 [hep-ph]].
- [93] V. Pascalutsa, M. Vanderhaeghen and S. N. Yang, Phys. Rept. **437**, 125 (2007) doi:10.1016/j.physrep.2006.09.006 [hep-ph/0609004].
- [94] C. B. Dover and A. Gal, Prog. Part. Nucl. Phys. **12**, 171 (1985) doi:10.1016/0146-6410(84)90004-8
- [95] R. Machleidt, Phys. Rev. C **63**, 024001 (2001) doi:10.1103/PhysRevC.63.024001 [nucl-th/0006014].
- [96] K. Nakamura *et al.* [Particle Data Group], J. Phys. G **37**, 075021 (2010). doi:10.1088/0954-3899/37/7A/075021